Search for gravitational waves from Scorpius X-1 in the second Advanced LIGO observing run with an improved hidden Markov model

B. P. Abbott *et al.*[*]
(LIGO Scientific Collaboration and Virgo Collaboration)

(Received 28 June 2019; published 4 December 2019)

We present results from a semicoherent search for continuous gravitational waves from the low-mass x-ray binary Scorpius X-1, using a hidden Markov model (HMM) to track spin wandering. This search improves on previous HMM-based searches of LIGO data by using an improved frequency domain matched filter, the $\mathcal{J}$-statistic, and by analyzing data from Advanced LIGO's second observing run. In the frequency range searched, from 60 to 650 Hz, we find no evidence of gravitational radiation. At 194.6 Hz, the most sensitive search frequency, we report an upper limit on gravitational wave strain (at 95% confidence) of $h_0^{95\%} = 3.47 \times 10^{-25}$ when marginalizing over source inclination angle. This is the most sensitive search for Scorpius X-1, to date, that is specifically designed to be robust in the presence of spin wandering.

DOI: 10.1103/PhysRevD.100.122002

I. INTRODUCTION

Rotating neutron stars with nonaxisymmetric deformations are predicted to emit persistent, periodic gravitational radiation. They are a key target for continuous-wave searches performed with gravitational wave (GW) detectors such as the second-generation Advanced Laser Interferometer Gravitational-Wave Observatory (Advanced LIGO) [1–5] and Virgo [4]. The time-varying quadrupole moment necessary for GW emission may result from thermal [6,7], or magnetic [8–10] gradients, r-modes [11–13], or nonaxisymmetric circulation of the superfluid interior [14–17]. These mechanisms produce signals at certain multiples of the spin frequency $f_\star$ [1]. Of particular interest are accreting low-mass x-ray binaries (LMXB), such as Scorpius X-1 (Sco X-1), where a neutron star is spun up by accretion from its stellar companion. Electromagnetic observations of LMXBs to date imply $f_\star \lesssim 620$ Hz [18], well short of the theoretical centrifugal break-up limit $f_\star \lesssim 1.5$ kHz [19]. Regardless of the exact GW mechanism, the latter observation suggests an equilibrium between the spin-up accretion torque, and GW spin-down torque [20–22]. Torque balance also implies a relation between x-ray luminosity and the GW strain, making Sco X-1, the brightest LMXB x-ray source, the most promising known target.

Initial LIGO, a first-generation detector, started taking science data in 2002. It reached its design sensitivity in Science Run 5 (S5) starting 2005 [23], and exceeded it in Science Run 6 (S6) [24]. Following detector upgrades, the second-generation Advanced LIGO interferometer [2] began taking science data during Observing Run 1 (O1), which ran from September 2015 to January 2016. The strain noise in O1 is 3 to 4 times lower than S6 between 100 and 300 Hz [25]. During this period, LIGO observed three binary black hole mergers, GW150914 [26], GW151012, and GW151226 [27]. Observing Run 2 (O2) began in November 2016, and ran until August 26, 2017. From August 1, 2017, the two LIGO detectors were joined by Virgo, resulting in a three-detector network. As well as further binary black hole mergers [28], LIGO and Virgo made the first gravitational wave observation of a binary neutron-star merger during O2 [29].

No search has yet reported a detection of a continuous-wave source. To date, four searches for Sco X-1 have been conducted on Initial LIGO data, and three on Advanced LIGO data. The first search coherently analyzed the most-sensitive six hour segment from Science Run 2 (S2) using the $\mathcal{F}$-statistic [30], a maximum-likelihood detection statistic [31]. The second was a directed, semicoherent analysis using the $\mathcal{C}$-statistic [32]. The third, also a directed analysis, used the TwoSpect algorithm on doubly Fourier transformed S5 data [33–35]. The fourth applied the radiometer algorithm [36] to conduct a directed search on S4 [37], S5 [38], and later O1 [39] data. Three LMXB searches have been performed with Advanced LIGO data, comprising the radiometer search [39], an analysis based on a hidden Markov model (HMM) [40], and a cross-correlation analysis [41–43]. The upper limits established by these searches are summarized in Table I.

Astrophysical modeling and x-ray observations suggest that the spin frequency of a LMXB wanders stochastically in response to fluctuations in the hydromagnetic accretion torque [46–49]. As no electromagnetic measurements of $f_\star$ are available to guide a gravitational wave search for Sco X-1, such searches must either account for spin wandering or limit their observing times and/or coherence

[*]Full author list given at the end of the article.

TABLE I. Summary of indicative upper limits achieved in previous searches for Sco X-1. VSR2 and VSR3 are Virgo Science Runs 2 and 3, respectively. Where applicable, the upper limits refer to signals of unknown polarization.

Search	Data	Upper limit	Reference
$\mathcal{F}$-statistic	S2	$h_0^{95\%} \lesssim 2 \times 10^{-22}$ at 464–484 Hz, 604–626 Hz	[31]
$\mathcal{C}$-statistic	S5	$h_0^{95\%} \lesssim 8 \times 10^{-25}$ at 150 Hz	[32]
TwoSpect	S6, VSR2, VSR3	$h_0^{95\%} \lesssim 2 \times 10^{-23}$ at 20–57.25 Hz	[34]
Radiometer	S4, S5	$h_0^{90\%} \lesssim 2 \times 10^{-24}$ at 150 Hz	[38, 44]
TwoSpect	S6	$h_0^{95\%} \lesssim 1.8 \times 10^{-24}$ at 165 Hz	[45]
Radiometer	O1	$h_0^{90\%} \lesssim 6.7 \times 10^{-25}$ at 130–175 Hz	[39]
Viterbi 1.0	O1	$h_0^{95\%} \lesssim 8.3 \times 10^{-25}$ at 106 Hz	[40]
Cross-correlation	O1	$h_0^{95\%} \lesssim 2.3 \times 10^{-25}$ at 175 Hz	[43]

times in accordance with the anticipated timescale and amplitude of the spin wandering [50]. For example, the sideband search described in Ref. [32] is restricted to data segments no longer than ten days. The HMM tracker, first applied to the search for Sco X-1 in Ref. [40], is an effective technique for detecting the most probable underlying spin frequency, $f_\star(t)$ and thus accounting for spin wandering.

The signal from a binary source is Doppler shifted, as the neutron star revolves around the barycenter of the binary, dispersing power into orbital sidebands near the source-frame emission frequency. The separation of these sidebands and the source-frame frequency depends on the binary orbital parameters and f, but is typically within 0.05% of the gravitational wave frequency for a source such as Sco X-1. Four maximum-likelihood matched filters have been developed to detect these sidebands: the $\mathcal{C}$-statistic, which weights sidebands equally [32], the binary modulated $\mathcal{F}$-statistic [51], the Bessel-weighted $\mathcal{F}$-statistic [52], and the $\mathcal{J}$-statistic, which extends the Bessel-weighted $\mathcal{F}$-statistic to account for the phase of the binary orbit [53]. Any of these matched filters can be combined with the HMM to conduct a search for signals from a binary source that accounts for spin wandering.

In this paper, we combine the $\mathcal{J}$-statistic described in Ref. [53] with the HMM described in that paper and Refs. [40, 50], and perform a directed search of Advanced LIGO O2 data for evidence of a gravitational wave signal from Sco X-1. In the search band 60–650 Hz, we find no evidence of a gravitational wave signal. The paper is organized as follows. In Sec. II, we briefly review the HMM and the $\mathcal{J}$-statistic. In Sec. III, we discuss the search strategy and parameter space. In Sec. IV, we report on the results from the search and veto candidates corresponding to instrumental artifacts. In Sec. V, we discuss the search sensitivity and consequent upper limits on the gravitational wave strain.

II. SEARCH ALGORITHM

In this section, we outline the two key components of the search algorithm: the HMM used to recover the most probable spin history $f_0(t)$, and the $\mathcal{J}$-statistic, the matched filter that accounts for the Doppler shifts introduced by the orbital motions of Earth and the LMXB. The HMM formalism is the same as used in Refs. [40,52,53], so we review it only briefly. The $\mathcal{J}$-statistic is described fully in Ref. [53]; again, we review it briefly.

A. HMM formalism

A Markov model describes a stochastic process in terms of a state variable $q(t)$, which transitions between allowable states $\{q_1, \ldots, q_{N_Q}\}$ at discrete times $\{t_0, \ldots, t_{N_T}\}$. The transition matrix $A_{q_j q_i}$ represents the probability of jumping from state q_i at the time $t = t_n$ to q_j at $t = t_{n+1}$ depending only on $q(t_n)$. A HMM extends the Markov model to situations where direct observation of $q(t)$ is impossible [$q(t)$ is called the hidden state]. Instead one measures an observable state $o(t)$ selected from $\{o_1, \ldots, o_{N_o}\}$, which is related to the hidden state by the emission matrix $L_{o_j q_i}$, which gives the likelihood that the system is in state q_i given the observation o_j. In gravitational wave searches for LMXBs like Sco X-1, where the spin frequency cannot be measured electromagnetically, it is natural to map $q(t)$ to $f_0(t)$ and $o(t)$ to the raw interferometer data, some equivalent intermediate data product (e.g., short Fourier transforms), or a detection statistic (e.g., $\mathcal{F}$-statistic, $\mathcal{J}$-statistic).

In a LMXB search, we divide the total observation (duration $T_{\rm obs}$) into N_T equal segments of length $T_{\rm drift} = T_{\rm obs}/N_T$. In practice, $T_{\rm drift}$ is chosen on astrophysical grounds to give $N_T = \lceil T_{\rm obs}/T_{\rm drift} \rceil$ based on an estimates of plausible spin-wandering timescales [50]; in this paper we follow Ref. [40] in choosing $T_{\rm drift} = 10$d. The tracker is able to track the signal even if the spin frequency occasionally jumps by two bins as it can catch up to the signal path, although with an attendant loss of sensitivity as the recovered must include a step that contains only noise.

In each segment, the emission probability $L_{o_j q_i}$ is computed from some frequency domain estimator $G(f)$ such as the maximum likelihood $\mathcal{F}$- or $\mathcal{J}$-statistic (discussed in Sec. II B). The frequency resolution of the

estimator is $\Delta f_{\rm drift} = 1/(2T_{\rm drift})$. The probability that an observation $O = \{o(t_1), \ldots, o(t_{N_T})\}$ is associated with a particular hidden path $Q = \{q(t_0), \ldots, q(t_{N_T})\}$ is then given by

$$P(Q|O) \propto L_{o(t_{N_T})q(t_{N_T})} A_{q(t_{N_T})q(t_{N_T-1})} \cdots L_{o(t_1)q(t_1)} \times A_{q(t_1)q(t_0)} \Pi_{q(t_0)}, \tag{1}$$

where Π_{q_i} is the prior, i.e., the probability the system starts in state q_i at $t = t_0$. For this search, we take a flat prior. [Note that there is no initial observation $o(t_0)$ as the initial state of the system is captured by the prior.] The task, then, is to find the optimal hidden path $Q^\star$, that is, the path $Q^\star$ that maximizes $P(Q|O)$ given O. We find $Q^\star$ efficiently with the recursive Viterbi algorithm [54], which is discussed in detail in Appendix A of Ref. [40].

In this paper, we follow the convention in Ref. [40] of defining the Viterbi detection score S for a path as the number of standard deviations by which that path's log-likelihood exceeds the mean log-likelihood of all paths. Mathematically we have

$$S = \frac{\ln \delta_{q^\star}(t_{N_T}) - \mu_{\ln \delta(t_{N_T})}}{\sigma_{\ln \delta(t_{N_T})}}, \tag{2}$$

where

$$\mu_{\ln \delta(t_{N_T})} = N_Q^{-1} \sum_{i=1}^{N_Q} \ln \delta_{q_i}(t_{N_T}), \tag{3}$$

$$\sigma^2_{\ln \delta(t_{N_T})} = N_Q^{-1} \sum_{i=1}^{N_Q} [\ln \delta_{q_i(t_{N_T})} - \mu_{\ln \delta(t_{N_T})}]^2, \tag{4}$$

$\delta_{q_i}(t_{N_T})$ denotes the likelihood of the most likely path ending in state q_i at step N_T, and $\delta_{q^\star}(t_{N_T}) = \max_i \delta_{q_i}(t_{N_T})$ is the likelihood of the optimal path overall.

B. $\mathcal{J}$-statistic

The frequency domain estimator $G(f)$ converts the interferometer data into the likelihood that a signal is present at frequency f. For a continuous-wave search for an isolated neutron star, the maximum-likelihood $\mathcal{F}$-statistic [30] is a typical choice for $G(f)$. The $\mathcal{F}$-statistic accounts for the diurnal rotation of Earth, and its orbit around the Solar System barycenter. It is an almost optimal matched filter for a biaxial rotor [55].

For a neutron star in a binary system, such as a LMXB, the signal is frequency (Doppler) modulated by the binary orbital motion as well. Reference [40] used the Bessel-weighted $\mathcal{F}$-statistic to account for this modulation, without using information about the orbital phase. Reference [53] introduced the $\mathcal{J}$-statistic, which is a matched filter that extends the $\mathcal{F}$-statistic to include orbital phase in the signal model. The orbital Doppler effect distributes the $\mathcal{F}$-statistic power into approximately $2m + 1$ orbital sidebands separated by P^{-1}, with $m = \lceil 2\pi f_\star a_0 \rceil$, where $\lceil \cdot \rceil$ denotes rounding up to the nearest integer, P is the orbital period, and $a_0 = (a \sin i)/c$ is the light travel time across the projected semimajor axis (where a is semimajor axis and i is the inclination angle of the binary). For a zero-eccentricity Keplerian orbit, the Jacobi-Anger identity may be used to expand the signal $h(t)$ in terms of Bessel functions, suggesting a matched filter of the form [52,53]

$$G(f) = \mathcal{F}(f) \otimes B(f), \tag{5}$$

with

$$B(f) = \sum_{s=-m}^{m} J_s(2\pi f_0 a_0) e^{-is\phi_a} \delta(f - s/P), \tag{6}$$

where $J_s(z)$ is the Bessel function of the first kind of order s, ϕ_a is the orbital phase at a reference time, and δ is the Dirac delta function.

All else being equal, using the $\mathcal{J}$-statistic instead of the Bessel-weighted $\mathcal{F}$-statistic improves sensitivity by a factor of approximately 4. Reference [53], particularly Sec. IV of that paper, examines the difference between the two estimators in depth.

The Bessel-weighted $\mathcal{F}$-statistic requires a search over a_0 but does not depend on ϕ_a. By contrast, the more-sensitive $\mathcal{J}$-statistic involves searching over ϕ_a too. In this paper we apply the $\mathcal{J}$-statistic to search for Sco X-1. Details of the search and priors derived from electromagnetic measurements are discussed in Sec. III.

III. LIGO O2 SEARCH

A. Sco X-1 parameters

The matched filter described in Sec. II B depends on three binary orbital parameters: the period P, the projected semimajor axis a_0, and the phase ϕ_a. The $\mathcal{F}$-statistic depends on the sky location α (right ascension) and δ (declination), and optionally the source frequency derivatives. For this search, we assume there is no secular evolution in frequency. The other parameters have been measured electromagnetically for Sco X-1 and are presented in Table II.

For α, δ, and P, the uncertainties in the electromagnetic measurements are small enough that they have no appreciable effect on the sensitivity of the search [51,60,61], and a single, central value can be assumed. However, the uncertainties in a_0 and ϕ_a cannot be neglected. The time spent searching orbital parameters scales as the number of (a_0, ϕ_a) pairs. Careful selection of the ranges of a_0 and ϕ_a is essential to keep computational costs low.

TABLE II. Electromagnetic measurements of the sky position and binary orbital parameters of Sco X-1. The uncertainties represent one-sigma (68%) confidence intervals, except for a_0, for which hard limits are given. The search resolution for a_0 and $T_{\rm asc}$ is different in each frequency subband, as discussed in Sec. III A. The search range for the time of ascension is the observed time of ascension propagated forward to the start of O2.

Observed parameter	Symbol	Value	Reference
Right ascension	α	16 h 19 m 55.0850 s	[56]
Declination	δ	$-15°38'24.9''$	[56]
Orbital period	P	68023.86048 ± 0.0432 s	[57]
Projected semimajor axis	a_0	[1.45, 3.25] s	[57]
Polarization angle	ψ	$234 \pm 3°$	[58]
Orbital inclination angle	i	$44 \pm 6°$	[58]
Time of ascension	$T_{\rm asc}$	974416624 ± 50 s	[57,59]

Search parameter	Symbol	Search range	Resolution
Frequency	f_0	60–650 Hz	5.787037×10^{-7} Hz
Projected semimajor axis	a_0	1.450–3.250 s	Variable
Time of ascension	$T_{\rm asc}$	1164543014–1164543614 s	Variable

The previous analysis described in Ref. [40] used the Bessel-weighted $\mathcal{F}$-statistic in place of the $\mathcal{J}$-statistic, and searched over a uniformly gridded range of a_0, where the grid resolution did not depend on frequency. However, the $\mathcal{J}$-statistic is more sensitive to mismatch in the binary orbital parameters, so a finer grid is required. We must also choose an appropriate grid for ϕ_a. (The Bessel-weighted $\mathcal{F}$-statistic is independent of ϕ_a.)

As the $\mathcal{J}$-statistic has a similar overall response to parameter mismatches as the binary $\mathcal{F}$-statistic, we follow the formalism in Ref. [51] to select an appropriate parameter space gridding. We choose a grid which limits the maximum loss in signal-to-noise ratio (mismatch) $\mu_{\rm max}$ to $\mu_{\rm max} = 0.1$. Equation (71) in Ref. [51] gives a general equation for the number of grid points needed for each search parameter. For the particular search considered in this paper, the number of choices for a_0 and ϕ_a are

$$N_{a_0} = \left\lceil \frac{\pi\sqrt{2}}{2} \mu_{\rm max}^{-1/2} f_0 \Delta a_0 \right\rceil, \tag{7}$$

$$N_{\phi_a} = \left\lceil \frac{1}{2} \mu_{\rm max}^{-1/2} f_0 a_0 \left(\frac{2\pi}{P}\right) \Delta\phi_a \right\rceil, \tag{8}$$

where Δa_0 and $\Delta\phi_a$ are the widths of the search ranges for a_0 and ϕ_a respectively. The number of orbital parameters to be searched depends on the search frequency. Accordingly for each search subband, we adopt a different grid resolution, with the grid refined at higher frequencies. In the subband beginning at 60 Hz, we have $N_{a_0} = 768$ and $N_{\phi_a} = 78$; in the subband beginning at 650 Hz, we have $N_{a_0} = 8227$ and $N_{\phi_a} = 824$. In principle we could achieve further computational savings by noting that N_{ϕ_a} also depends on a_0, but for safety we use the largest a_0.

The search range for a_0 is $1.45 \leq a_0/(1\ \text{s}) \leq 3.25$, which matches the most recent electromagnetic measurement [57] and widens the error bars on the widely cited and previous best published measurement, $a_0 = 1.44 \pm 0.18$ s [62].

The orbital phase ϕ_a can be related to the electromagnetically measured time of ascension, $T_{\rm asc}$, given in Table II, by

$$\phi_a = 2\pi T_{\rm asc}/P \pmod{2\pi}. \tag{9}$$

The one-sigma uncertainty in the published value for $T_{\rm asc}$ is ± 50 s [57,59] for a time of ascension at GPS time 974416624 s (in November 2010). As O2 took place significantly after this time, to make a conservative estimate on appropriate error bars for $T_{\rm asc}$, we advance $T_{\rm asc}$ by adding 3135 orbital periods to the time of ascension taken from Ref. [57]. As there is uncertainty associated with the measured orbital period, this widens the one-sigma uncertainty of $T_{\rm asc}$ to ± 144 s, which we round up to ± 150 s. To cover a significant portion of the measured $T_{\rm asc}$ range while keeping the search computationally feasible, we search a two-sigma range around the central $T_{\rm asc}$, namely, $1164\,543\,014 \leq T_{\rm asc}/(1\ \text{s}) \leq 1\,164\,543\,614$ (expressed for presentation purposes as the time of the last ascension before the start of O2).

As there is no electromagnetic measurement of $f_\star$ for Sco X-1, we search the band $60 \leq f_\star/(1\ \text{Hz}) \leq 650$, where LIGO is most sensitive, again adopting a uniform prior (see Sec. II A for a discussion of the HMM prior). The same band is analyzed in Ref. [40]. For computational convenience, we split the band into blocks of approximately 0.61 Hz (discussed further in Sec. III B).

The final electromagnetically measured parameter is the polarization angle, ψ. Because the $\mathcal{F}$-statistic components of the $\mathcal{J}$-statistic are maximized over the polarization angle, the $\mathcal{J}$-statistic is insensitive to ψ.

A summary of the search ranges flowing from the electromagnetically measured parameters of Sco X-1 is presented in Table II.

B. Workflow

The workflow for the search is displayed as a flowchart in Fig. 1.

The data from the detector are provided as short Fourier transforms (SFTs), each covering $T_{\mathrm{SFT}} = 1800$ s. We divide the search into subbands, both to facilitate managing the volume of data, and to ensure that replacing the search frequency f with the midpoint of the subband, $\bar{f}$, is a good approximation in Eq. (6). To achieve best performance from the fast Fourier transforms used to compute the convolution in (6), it is desirable to have a power of 2 number of frequency bins in the band, so we set the subband width to be $\Delta f_{\mathrm{band}} = 2^{20}\Delta f_{\mathrm{drift}} = 0.6068148$ Hz. This in turn sets the number of hidden states per subband per binary orbital parameter to be $N_Q = 2^{20}$.

For each subband, we divide the data into N_T blocks, each with duration $T_{\mathrm{drift}} = 10$ d. We then compute, from the SFTs, the $\mathcal{F}$-statistic "atoms" [63] ($\mathcal{F}_a$, $\mathcal{F}_b$) for each block using the fixed parameters (α, δ, P) in Table II.

The next step is to compute the $\mathcal{J}$-statistic for the (a_0, ϕ_a) search grid described in Sec. III A. The $\mathcal{F}$-statistic atoms do not depend on the binary orbital parameters so they are not recomputed when calculating the $\mathcal{J}$-statistic. The code to compute the $\mathcal{J}$-statistic is based on the $\mathcal{F}$-statistic subroutines contained in the LIGO Scientific Collaboration Algorithm Library [64].

After computing the $\mathcal{J}$-statistic, we use the Viterbi algorithm to compute the optimal paths through the HMM trellis, i.e., the set of vectors $Q^\star$. In principle, the tracking problem is three dimensional (over f_0, a_0, and ϕ_a), but a_0 does not vary significantly over $T_{\mathrm{obs}} \lesssim 1$ yr and ϕ_a varies deterministically, with the phase at time step n given by $\phi_a(t_n) = \phi_a(t_{n-1}) + 2\pi T_{\mathrm{drift}}/P$. Thus, it is convenient to search independently over f_0 and pairs (a_0, ϕ_a). This allows searches over (a_0, ϕ_a) pairs to be performed in parallel.

The result of this procedure is one log-likelihood for the optimal path through the trellis terminating at every 3-tuple (f_0, a_0, ϕ_a). Equation (2) converts these log-likelihoods to Viterbi scores. As the noise power spectral density (PSD) of the detector is a function of f_0, we compute μ and σ separately for each band. By contrast, the PSD is not a function of a_0 and ϕ_a. Therefore, we can recalculate μ and σ for every (a_0, ϕ_a) pair (rather than calculating μ and σ using every log-likelihood across the entire search), thereby considerably reducing memory use. This has no significant impact on the Viterbi scores.

For each subband that produces a best Viterbi score lower than the detection threshold (chosen in Sec. III C), we compute an upper limit on the gravitational wave strain for a source in that subband. For Viterbi scores that exceed the threshold, we apply the veto tests described in Sec. IV A. We claim a detection, if a candidate survives all vetoes.

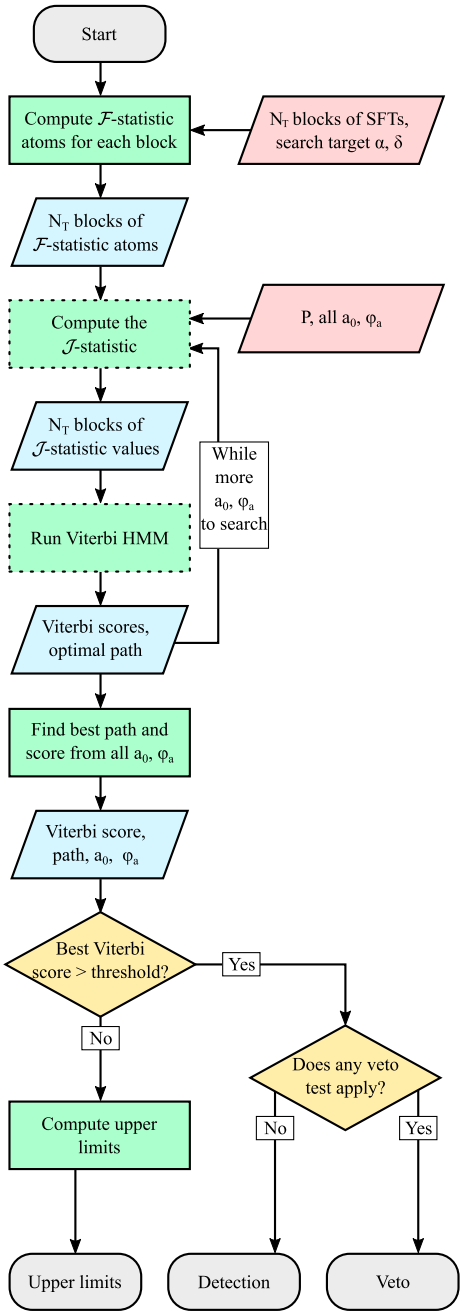

FIG. 1. Flowchart of the $\mathcal{J}$-statistic search pipeline for each subband. Note that the $\mathcal{F}$-statistic atoms are computed once per block and per subband, then the $\mathcal{J}$-statistic is recalculated for each (a_0, ϕ_a) pair. The gray ovals are the start and end of the algorithm, the green rectangles are procedures, the blue (red) parallelograms are intermediate (input) data, the yellow diamonds are decision points, and the gray dashed line represents a loop repeated once for each choice of parameter. The rectangles with a dashed boundary were run on graphical processing units, while those with a solid boundary were run on central processing units.

For performance reasons, the most computationally intensive parts of the search (computing the $\mathcal{J}$-statistic,

and the Viterbi tracking) were run using NVIDIA P100 graphical processing units (GPUs). Other steps were run using CPU codes on Intel Xeon Gold 6140 CPUs.

C. Threshold and false alarm probability

It remains to determine a detection score threshold $S_{\rm th}$ corresponding to the desired false alarm probability. Consider the probability density function (PDF) $p_{\rm n}(S)$ of the Viterbi score in noise. For a given threshold $S_{\rm th}$ and a fixed search frequency and set of binary orbital parameters, the probability that the score will exceed this threshold (i.e., produce a false alarm) is

$$\alpha = \int_{S_{\rm th}}^{\infty} {\rm d}S p_{\rm n}(S). \tag{10}$$

In general, the search covers many frequency bins and choices of binary parameters. The probability α_N of a false alarm over a search covering N parameter choices (number of frequency bins multiplied by number of binary parameter choices) is

$$\alpha_N = 1 - (1-\alpha)^N. \tag{11}$$

This equation assumes that the Viterbi score in noise is an independent random variable at each point in the parameter space, which is not necessarily true, as the $\mathcal{J}$-statistic calculated for two points nearby in parameter space is correlated to some degree. However, for $\mu_{\rm max} = 0.1$ as used in this search, these correlations do not have a significant impact [65]. In practice, we fix α_N and N and solve (10) and (11) for α and hence $S_{\rm th}$.

As the noise-only PDF $p_{\rm n}(S)$ of the Viterbi score is unknown analytically [40], we resort to Monte Carlo simulations. We generate 10^2 Gaussian noise realizations in seven subbands of width $\Delta f_{\rm band}$, namely those starting at 55, 155, 255, 355, 455, 555, and 650 Hz. The noise is generated using the standard LIGO tool lalapps_Makefakedata_v4. These are the same subbands used in Sec. III C of Ref. [40], and the one-sided noise PSD $S_h(f)$ is set to match the O2 data. We then perform the search described in Sec. III B (including scanning over a_0 and ϕ_a).

The results of this search produce an empirical version of $p_{\rm n}(S)$. Plotting the tail of this distribution on a logarithmic plot suggests that a fit to a function of the form $e^{\lambda S}$ is an appropriate choice to allow the PDF to be extrapolated in order to solve (11).

We first analyze each band independently to ensure that there is no frequency dependence in $p_{\rm n}(S)$. Table III gives the best-fit λ, and the threshold $S_{\rm th}$ obtained, for each band analyzed in isolation. We find that there is no significant dependence on the subband searched, nor any identifiable trend in λ or $S_{\rm th}$. Combining the realizations for all bands produces $\lambda = -3.28$ and hence $S_{\rm th} = 13.66$ for $\alpha = 0.01$.

TABLE III. Results of investigating the empirical PDF of the Viterbi score in seven subbands in Gaussian noise. The second column is λ obtained by fitting the PDF to $e^{\lambda S}$. The third column is the threshold $S_{\rm th}$ obtained by solving Eq. (11).

Start of band (Hz)	λ	$S_{\rm th}$
55	−3.02	14.12
155	−3.24	13.63
255	−3.26	13.58
355	−3.27	13.61
455	−3.30	13.62
555	−3.29	13.66
650	−3.29	13.63

The empirical PDF and fitted exponential are shown in Fig. 2.

D. Sensitivity

After selecting $S_{\rm th}$, it remains to determine the lowest (as a function of frequency) characteristic wave strain, $h_0^{95\%}$, that can be detected with 95% efficiency (i.e., a 5% false dismissal rate). To do this, we generate Monte Carlo realizations of Gaussian noise with Sco X-1–like signals injected. We determine the proportion of signals recovered as a function of h_0 and double-check the false alarm probability quoted above.

For O2, the most sensitive subband of width $\Delta f_{\rm band} = 0.6068148$ Hz is the one beginning at 194.6 Hz. Following a typical procedure used to find upper limits for continuous gravitational wave searches [66], we generate 10^2 noise realizations and inject signals using the source parameters in Table II, with $T_{\rm obs} = 230$ d (the duration of O2), $T_{\rm drift} = 10$ d, $N_T = 23$, $\sqrt{S_h} = 7.058 \times 10^{-24}$ Hz$^{-1/2}$, and $\cos\iota = 1$. The remaining range-bound parameters, namely $f_{0_{\rm inj}}$, $a_{0_{\rm inj}}$, $T_{{\rm asc}_{\rm inj}}$, and $\psi_{\rm inj}$ are chosen from a uniform

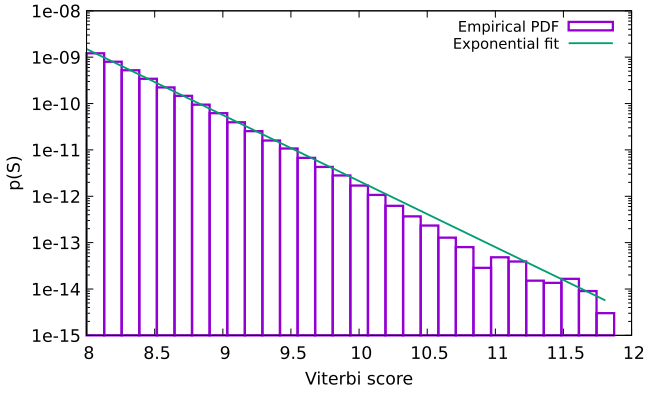

FIG. 2. Tail of the PDF of the Viterbi score S in noise. The purple histogram shows the empirical PDF derived from 10^2 realizations of the noise analyzed in the seven 0.61 Hz subbands starting at 55, 155, 255, 355, 455, 555, and 650 Hz. The green curve is an exponential fitted to the histogram.

distribution within the range given by their one σ error bars. The source frequency $f_{0_{\mathrm{inj}}}$ is chosen from a uniform distribution on the interval [194.6 Hz, 194.7 Hz]. For each realization, the signal is injected with progressively lower h_0 until it can no longer be detected. We denote by $h_{0,\mathrm{min};i}$ the lowest h_0 that can be detected in realization i. To obtain $h_0^{95\%}$, we take the 95th highest $h_{0,\mathrm{min};i}$. The simulations return the threshold $h_0^{95\%} = 1.46 \times 10^{-25}$ at 194.6 Hz.

In general, the signal-to-noise ratio is strongly affected by the inclination angle ι, not just h_0. We follow Ref. [59] and define an effective h_0 that absorbs the dependence on ι:

$$h_0^{\mathrm{eff}} = h_0 2^{-1/2}\{[(1+\cos^2\iota)/2]^2 + \cos^2\iota\}^{1/2}, \quad (12)$$

allowing us to generalize results from the simulations above, where all injections were done with $\cos\iota = 1$. Thus, the result obtained above corresponds to circular polarization. The electromagnetically measured inclination of Sco X-1's orbit is $i \approx 44° \pm 6°$ [58]. Although it is not necessarily the case, if we assume that the orbital inclination equals the inclination angle ι of the putative neutron star's spin axis, we obtain $h_0^{\iota\approx 44°,95\%} = 1.35 h_0^{\mathrm{eff},95\%}$.

The search in Ref. [40] found a scaling relation of the form $h_0^{95\%} \propto S_h^{1/2} f_0^{1/4}$ to hold for fixed T_{obs}. The $f_0^{1/4}$ dependence arises because the latter search added sidebands incoherently. In the case of the $\mathcal{J}$-statistic, which adds sidebands coherently, we expect the scaling to depend just on h_0, with

$$h_0^{95\%} \propto S_h^{1/2}. \quad (13)$$

We verify this scaling in Gaussian noise by repeating the injection procedure described above in frequency bands beginning at 55, 355, and 650 Hz. The scaling is the final ingredient needed to produce the blue dashed curve in Fig. 3, which shows the expected sensitivity of a search over the full search band, assuming Gaussian noise, a 100% duty cycle, and a circularly polarized signal.

There is no simple scaling similar to (13) that can be used to account for the effect of non-Gaussian noise and the detector duty cycle. Hence we introduce a multiplicative correction factor κ_j for a selection of subbands indexed

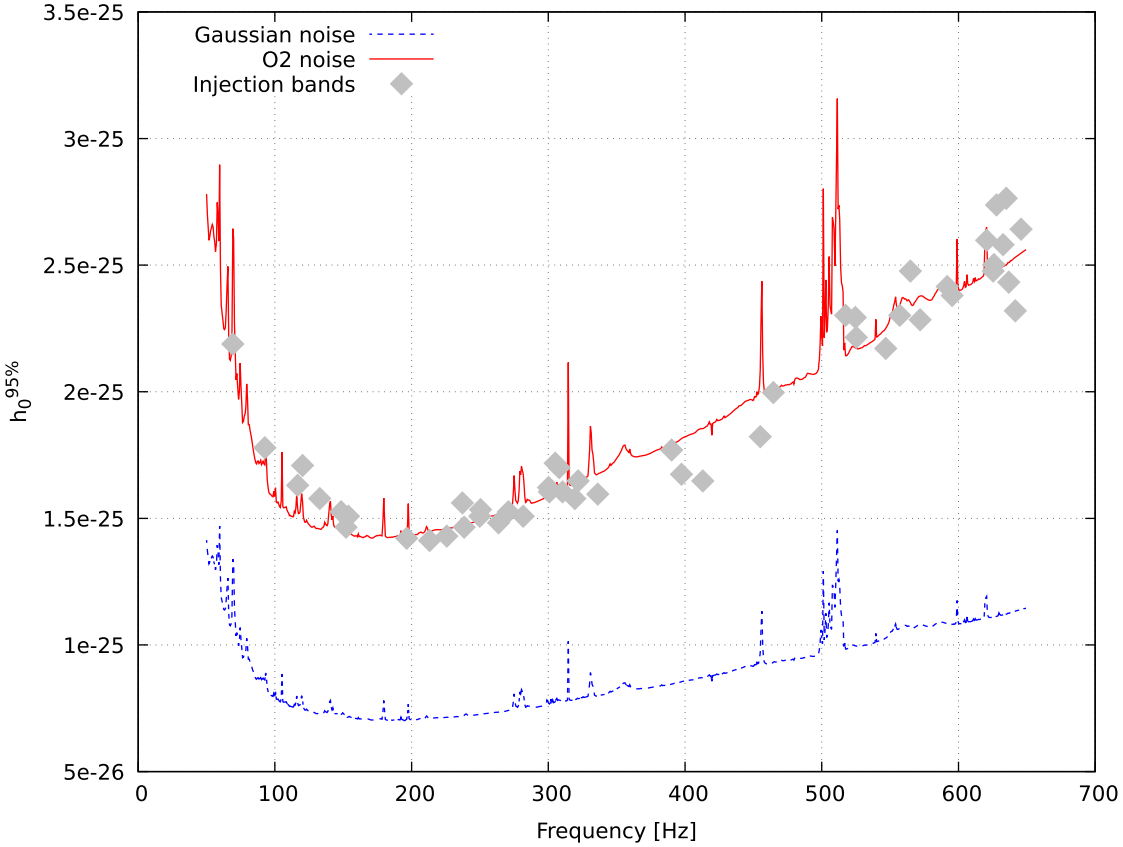

FIG. 3. Sensitivity of a search for Sco X-1 across the frequency band searched in this work. The horizontal axis shows the search frequency. The vertical axis shows the wave strain $h_0^{95\%}$ needed for a 95% detection efficiency, on the assumption $\cos\iota = 1$, namely, a circularly polarized signal. The blue dashed curve is based on simulations of Gaussian noise, while the red solid curve is corrected for the non-Gaussian statistics of the noise and the interferometer duty cycle, through multiplying by $\kappa_{\mathrm{freq}}(f)$ (see Sec. III D). The diamonds show $h_0^{95\%}$ derived through injections into subbands, again assuming a circularly polarized signal (see Sec. III D).

by j, following Ref. [40]. We determine κ_j by doing 10^2 injections (drawing parameters as described above) into the detector data for the jth subband, again using progressively lower h_0 until we determine the minimum h_0 detected. Then, κ_j equals $h_0^{\mathrm{eff},95\%}$ for injections into real noise, divided by $h_0^{\mathrm{eff},95\%}$ for injections into Gaussian noise.

Producing κ_j in this way for a random selection of subbands in the search band suggests that κ depends weakly on frequency, most likely due to the $\mathcal{J}$-statistic not perfectly summing sidebands [40]. A linear fit to the computed κ_j values suggests a frequency-dependent correction factor

$$\kappa_{\mathrm{freq}}(f) = 1.944 + 4.60 \times 10^{-4} f/(1\ \mathrm{Hz}). \quad (14)$$

We use $\kappa_{\mathrm{freq}}(f)$ to adjust the blue dashed curve in Fig. 3, producing the red solid curve in that figure, which represents the expected sensitivity across the full search band, where the noise is realistic (i.e., not Gaussian). The 50 subbands sampled are shown on the plot as gray diamonds.

IV. O2 ANALYSIS

We now analyze the data from LIGO's O2, using the full dataset from November 30, 2016 to August 26, 2017, including data from the LIGO Livingston (L1) and Hanford (H1) observatories. The Virgo interferometer also participated in the last two months of O2, but we do not use any Virgo data in this analysis.

There are two notable pauses in data gathering: an end-of-year break starting on December 22, 2016 lasting for 13 days, and a commissioning break starting on May 7, 2017 lasting for 19 (L1) or 32 (H1) days.

Data stretches shorter than T_{SFT} are discarded, as is a period of approximately one month where much of the band was contaminated due to a blinking light in the power system and a digital camera (used for detector diagnostics) that was inadvertently left on. A detailed discussion of Advanced LIGO detector noise can be found in Ref. [67]. Taking all these factors into account, the overall duty cycle (i.e., proportion of time spent gathering science-quality data) for O2 was 51.9% (L1) and 46.2% (H1).

Because of the commissioning break, one ten-day block has no data. We fill this block with a uniform log-likelihood, so that the HMM has no preference for remaining in the same frequency bin, or moving by one bin, during the break, while still allowing a maximum drift of $\Delta f_{\mathrm{drift}}$ every ten days. An alternative, but equivalent, approach would be to remove the break entirely, and alter the transition matrix $A_{q_i q_j}$ for that step to allow the HMM to wander up to two frequency bins. The end-of-year break is also longer than ten days, but it is covered by two blocks. Both of the blocks that overlap with the end-of-year break contain data.

We search the same frequency band as Ref. [40], namely 60–650 Hz. The lower limit is set by LIGO's poor sensitivity for signals $\lesssim$25 Hz and the significant contamination from instrumental noise in the band 25–60 Hz. The sensitivity of the search falls as frequency increases, while compute time rises dramatically. We terminate the search at 650 Hz, as in Ref. [40].

The results of the search are presented in Fig. 4, which shows the frequency and recovered orbital parameters a_0 and ϕ_a for every path with $S > S_{\mathrm{th}}$. The color of the points shows the Viterbi score associated with that path. As the

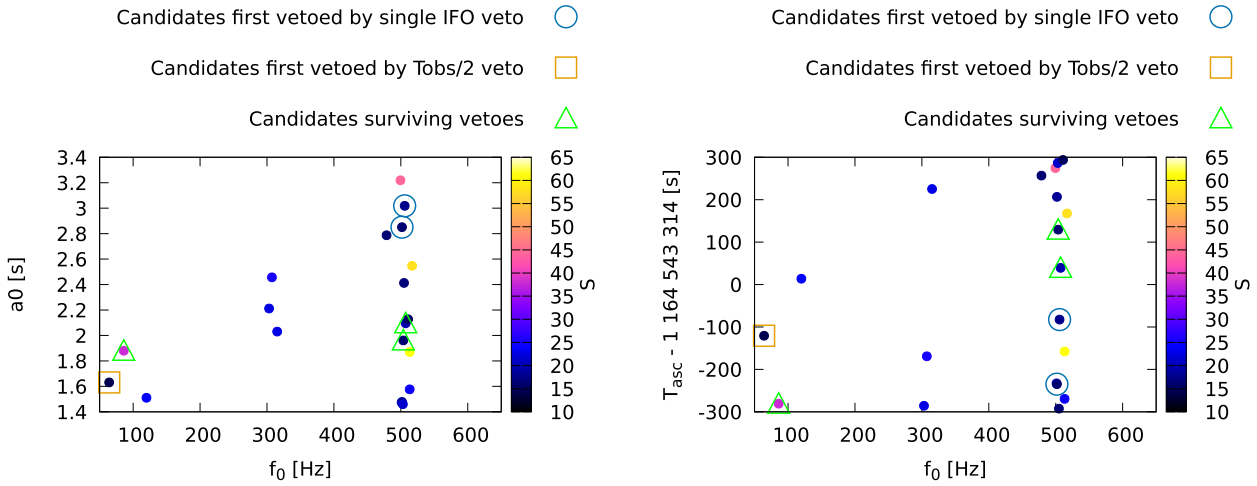

FIG. 4. Candidates identified by the search. The left-hand panel plots the detection score S (indicated by color; see color bar) as a function of final frequency $f_0(t_{N_T})$ (horizontal axis) and orbital semimajor axis a_0 (vertical axis) recovered by the HMM. The right-hand panel plots the candidates with T_{asc} on the vertical axis. Undecorated candidates are eliminated by the known line veto, candidates marked by blue circles are eliminated by the single-interferometer veto, candidates marked by orange squares are eliminated by the $T_{\mathrm{obs}}/2$ veto, and the candidates marked by green triangle survive the veto process.

most a signal can wander during the observation is $N_T \Delta f_{\rm drift} \approx 1.3 \times 10^{-5}$ Hz, which is small compared to $\Delta f_{\rm band}$ (and what can be visually discerned on Fig. 4), we define f_0 for a given path to be equal to $f_0(t = N_T)$ for convenience.

To rule out false alarms, we apply the hierarchy of vetoes first described in Ref. [40]. The vetoes are (1) the known instrumental lines veto (described in Sec. IV A 1 below), (2) the single-interferometer veto (Sec. IV A 2), (3) the $T_{\rm obs}/2$ veto (Sec. IV A 3), and (4) the $T_{\rm drift}$ veto (ultimately not used, but discussed in Sec. IV A 4 of Ref. [40]). To ensure that the vetoes are unlikely to falsely dismiss a true signal, we perform the search on a dataset with synthetic signals injected into it, and ensure that those injections are not vetoed. These veto safety tests are described in Sec. IV B.

The number of candidates found in the initial search, and then vetoed at each step, are listed in Table IV.

A. Vetoes

1. Known lines veto

There are a large number of persistent instrumental noise lines identified as part of LIGO's detector characterization process [67,68]. These lines can arise from a number of sources, including interference from equipment around the detector, resonant modes in the suspension system, and external environmental causes (e.g., the electricity grid).

A noise line generally produces high $|\mathcal{F}_a|$ and $|\mathcal{F}_b|$ values. The convolution in (6) reduces the impact of this somewhat by summing bins near and far from the line, but in practice the noise lines are strong enough that they contaminate any candidate nearby. Accordingly, we veto any candidate whose Viterbi path $f_0(t)$ satisfies $|f_0(t) - f_{\rm line}| < 2\pi a_0 f_0/P$, for any time t along the path and for any line frequency $f_{\rm line}$. This veto is efficient, excluding 14 of the 20 candidates.

2. Single interferometer veto

During O2, L1 was slightly more sensitive than H1, but overall the sensitivities of the two interferometers were similar. Accordingly, any astrophysical signal that can be detected in the combined dataset should either be detected by the individual detector datasets when analyzed separately (for stronger signals) or in neither (for weaker signals). A signal that is detectable in one interferometer only is likely to be a noise artifact, so we veto it.

Following Ref. [40], we compare the Viterbi scores obtained from individual detectors to the original combined score $S_\cup$ to classify survivors of the known line veto into four categories discussed below, one of which is vetoed.

Category A.—One detector returns $S < S_{\rm th}$, while the other detector returns $S > S_\cup$, and the frequency estimated by the latter detector is close to that of the original candidate $f_{0\cup}$, that is, $|f_{0\cup} - f_0| < 2\pi a_{0\cup} f_{0\cup}/P$, where the subscript $\cup$ denotes a quantity estimated by the search in both detectors. This category and the next represent signals where the score is dominated by one detector. We veto candidates in category A.

Category B.—As with category A, one detector returns $S < S_{\rm th}$, while the other detector returns $S > S_\cup$. Unlike category A, the frequency estimated by the latter detector is far from the original candidate, i.e., $|f_{0\cup} - f_0| > 2\pi a_{0\cup} f_{0\cup}/P$. In this case, it is possible that there is signal at $f_{0\cup}$ which is detectable when combining the data from both detectors but not from one detector, because an artifact masks its presence. Hence we keep the candidate for follow-up.

Category C.—The candidate is seen with $S > S_{\rm th}$ in both detectors. This could either be a relatively strong signal, or an artifact from a noise source common to both detectors. The single-interferometer veto cannot distinguish these possibilities. Again, we keep the candidate for follow-up.

Category D.—The candidate is not seen by either detector, with $S < S_{\rm th}$ in both detectors. This could be a signal that is too weak to see in either detector individually. We keep the candidate for follow-up.

Category A of the single-interferometer veto eliminates two of the remaining six candidates. The two eliminated candidates were stronger in H1 compared to L1.

TABLE IV. Number of candidates found in the first pass, and number remaining after applying the vetoes described in Sec. IV A.

After veto	Survivors
First pass	20
Line	6
Single interferometer	4
$T_{\rm obs}/2$	3

3. $T_{\rm obs}/2$ veto

We divide the observing run into two segments, the first covering 140 days from November 30, 2016 (GPS timestamp 1164562334) to April 19, 2017 (GPS timestamp 1176658334), and the second covering 90 days from January 19, 2017 (GPS timestamp 1168882334) to August 25, 2017 (GPS timestamp 1187731792). This division is chosen to get approximately equal effective observing time in the two segments. There is no forceful evidence to suggest that the gravitational wave strength of a LMXB varies significantly with time (and a signal with time-varying strength is likely to have a considerably more complicated form than assumed here); thus we do not expect a signal to appear preferentially in either segment. We search the segments separately for the candidates which survived both preceding vetoes. To determine whether to veto candidates at this stage, we apply the same set of categories as in veto 2.

This veto eliminates one remaining candidate, which is much stronger in the first segment of the observing run than the second.

Reference [40] describes the T_{drift} veto as a fourth veto that can be applied to candidates surviving the $T_{\mathrm{obs}}/2$ veto. However, this veto is applicable to candidates with an observed spin-wandering timescale that is 20 days or longer. This is not the case for the surviving three candidates, so the T_{drift} veto is not applicable to them.

The remaining candidates are in the subbands starting at 85.4, 503.6, and 507.2 Hz. The scores relevant to performing the veto procedure are given in Table V. All three candidates are stronger when analyzing the H1 detector data alone compared to analyzing L1 detector data alone, with the L1 results consistent with noise. The candidates in the subbands starting at 85.4 and 507.2 Hz are both stronger during the second half of O2 compared to the first half, while the candidate in the subband starting at 503.6 Hz is stronger in the analysis of the first half of O2. Particularly for the candidate in the 85.4 Hz subband, the asymmetry in score between the first and second half of the observing is extreme and suggestive of a detector artifact rather than an astrophysical signal. The asymmetry is less pronounced for the candidates in the subbands starting at 503.6 and 507.2 Hz, but both of these candidates are in a region of frequency space that is significantly contaminated by interferometer noise, particularly violin modes associated with the LIGO mirror suspension. For these reasons, it is most likely that these candidates are due to unknown instrumental noise in the H1 detector, although they are not formally ruled out by the veto procedure described above.

B. Veto safety

To verify that the vetoes described previously do not unduly increase the false dismissal probability, we inject signals into the O2 data and perform the veto procedure described in the previous section. We inject a total of 50 signals into 50 subbands of width Δf_{band} chosen to be comparable to the 200 injections used for the equivalent tests in Ref. [40] while having a large enough sample to be confident that false dismissals caused by the vetoes are rare in the context of the 5% false dismissal rate used in calculating sensitivity. The subbands and parameters chosen are selected randomly from the search band to achieve good frequency coverage, but excluding those subbands that contain a known line (and hence would be excluded by the known lines veto). Into these subbands, we inject a signal near the detection limit with h_0 typically at $h_0^{95\%}$ for that subband (although we inject a stronger signal if the signal turns out to be undetectable), and with f_0 drawn randomly from a uniform distribution over the interval $[f_{\mathrm{start}} + 0.1\ \mathrm{Hz}, f_{\mathrm{start}} + \Delta f_{\mathrm{band}} - 0.1\ \mathrm{Hz}]$, where f_{start} is the lowest frequency in the subband. At each block, the signal is allowed to wander at most one frequency bin (i.e., by an amount drawn uniformly from $[-\Delta f_{\mathrm{drift}}, +\Delta f_{\mathrm{drift}}]$), and the signal frequency is constant within the block, following Ref. [40]. The other parameters are chosen in the same way as for the sensitivity tests described in Sec. III D.

We then apply vetoes 2 (single-interferometer veto) and 3 ($T_{\mathrm{obs}}/2$ veto) to each candidate (veto 1 is inapplicable, as the injection bands avoid known lines, and veto 4 [T_{drift} veto] was not used in this search). No injection was vetoed.

Because the veto safety procedure uses the O2 data as noise, it is possible that the safety results described above depend in some way on the specifics of O2. However, as the veto procedure copies the equivalent procedure in Ref. [40], which tests both S5 noise and O1 noise, we have confidence that the veto safety result is not specific to the peculiarities of O2.

TABLE V. Viterbi scores of the three candidates that survived the veto procedure. The original score is the score of the original candidate from the search on the full O2 dataset. The H1 and L1 scores are the scores for the candidate when searching on each detector independently. The first and second part scores are the scores when analyzing the first 140 and last 90 days of the dataset, respectively.

Subband containing candidate	Original score	H1	L1	First part	Second part
85.4	42.4	30.7	6.3	7.2	41.8
503.6	41.3	34.6	5.8	37.5	6.1
507.2	17.3	10.6	6.1	10.2	16.4

V. UPPER LIMITS

We can use the nondetection reported in the previous section, in concert with the approach outlined in Sec. III D, to place an upper limit on h_0 as a function of f_0 and compare the result to the indirect, torque-balance upper limit established by the x-ray flux [20].

A. Frequentist upper limit at 95% confidence

Failure to detect a gravitational wave signal allows us to place an upper limit on h_0 from a particular source, given a desired confidence level. In this section, we follow Ref. [40] in using a frequentist approach and setting 95% as the desired confidence level. The alternative, Bayesian approach in Ref. [61] is hard to adapt to the HMM-based search, because correlations between the Viterbi paths render the distribution of Viterbi scores difficult to calculate analytically.

We define $h_0^{95\%}$ to be the lowest amplitude signal for which we have a 95% probability or greater of detecting a signal with $h_0 \geq h_0^{95\%}$, that is, $\Pr(S \geq S_{\mathrm{th}} | h_0 \geq h_0^{95\%}) \geq 0.95$. The value of $h_0^{95\%}$ depends on the inclination angle of the source, through Eq. (12). Figure 5 show the upper limit for three cases: assuming the neutron-star spin axis inclination

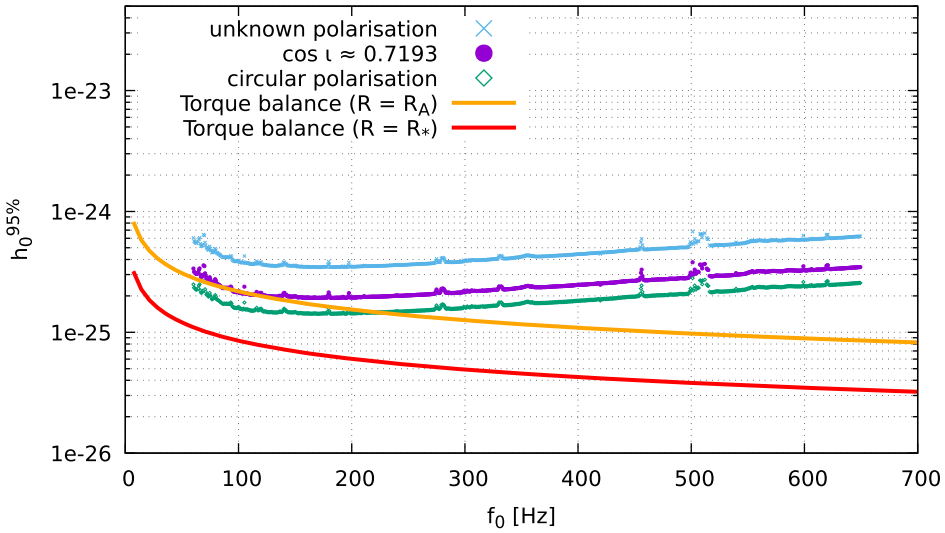

FIG. 5. Wave strain upper limits at 95% confidence as a function of signal frequency, corresponding to the frequentist upper limit in each subband (width $\Delta f_{\rm band}$), for three scenarios: a flat prior on $\cos\iota$ (blue crosses), the orientation $\iota \approx 44°$ derived from observations of the radio jet (filled purple circles), and the most optimistic case of circularly polarized waves (open green diamonds). These are compared to the indirect torque-balance upper limit, where the accretion torque is applied at the Alfvén radius (solid orange curve) or the stellar radius (solid red curve).

angle ι is equal to the electromagnetically constrained orbital inclination angle $i \approx 44°$ (purple plus signs), a pure circularly polarized signal $|\cos\iota| = 1$ (green crosses), and a flat prior on $\cos\iota$ (blue asterisks). For subbands with no candidate path with a Viterbi score above the threshold, we take $h_0^{95\%}$ from Fig. 3 for the circularly polarized case, and determine $h_0^{95\%}$ for the two other cases using Eq. (12). No upper limit is established for subbands containing a vetoed candidate (because those bands are deemed to be contaminated by instrumental artifacts). Accordingly those subbands are excluded from Fig. 5.

The circularly polarized case produces the most stringent upper limit reflecting the fact that $|\cos\iota| = 1$ would be the most favorable configuration for producing gravitational waves. Conversely, assuming no knowledge of the inclination angle (the flat prior case) produces a looser upper limit. The lowest upper limit for this search is in the subband starting at 194.6 Hz, with upper limits of $h_0^{95\%} = 3.47 \times 10^{-25}$, 1.93×10^{-25}, 1.42×10^{-25} for the unknown polarization, electromagnetically constrained, and circularly polarized cases, respectively. Previous work with the HMM in Ref. [40] found $h_0^{95\%} = 8.3 \times 10^{-25}$, 4.0×10^{-25}, 3.0×10^{-25} for those cases in its most sensitive subband starting at 106 Hz.

B. Torque-balance upper limit

An indirect upper limit on gravitational wave strain can be obtained from x-ray observations. If the spin-down torque due to gravitational wave emission balances the accretion spin-up torque, with the latter inferred from the x-ray luminosity, one has $h_0 \geq h_0^{\rm eq}$ with [20,22,60]

$$h_0^{\rm eq} = 5.5 \times 10^{-27} \left(\frac{F_X}{10^{-8}\ \mathrm{erg\,cm^{-1}\,s^{-1}}}\right)^{1/2} \left(\frac{R}{10\ \mathrm{km}}\right)^{3/4} \times \left(\frac{1.4\ M_\odot}{M_\star}\right)^{1/4} \left(\frac{300\ \mathrm{Hz}}{f_\star}\right)^{1/2}, \quad (15)$$

where F_X is the x-ray flux, R is the length of the notional "lever arm" to which the accretion torque is applied, $M_\star$ is the stellar mass, and $f_\star$ is the (unknown) spin frequency.

To establish an upper limit, we take the electromagnetically measured $F_X = 4 \times 10^{-7}$ erg cm^{-2} s^{-1} [49] of Sco X-1, and the common fiducial neutron-star mass $M_\star = 1.4\ M_\odot$. The most conservative choice for the accretion torque lever arm is the stellar radius $R_\star = 10$ km. We plot $h_0^{\rm eq}$ as a function of frequency as the solid red curve in Fig. 5. Another physically reasonable choice of lever arm length is the Alfvén radius, R_A, i.e., the distance out to which outflowing material corotates with the star's magnetic field. This is given by [40,48]

$$R_A = 35 \left(\frac{B_\star}{10^9\ \mathrm{G}}\right)^{4/7} \left(\frac{R_\star}{10\ \mathrm{km}}\right)^{12/7} \times \left(\frac{1.4\ M_\odot}{M_\star}\right)^{1/7} \left(\frac{10^{-8}\ M_\odot\,\mathrm{yr}^{-1}}{\dot{M}}\right)^{2/7} \mathrm{km}, \quad (16)$$

where $B_\star$ is the polar magnetic field strength at the stellar surface, G is Newton's gravitational constant, and $\dot{M}$ is the accretion rate. The accretion rates in LMXBs can range from the Eddington limit, $2 \times 10^{-8}\ M_\odot\,\mathrm{yr}^{-1}$, down to about $10^{-11}\ M_\odot\,\mathrm{yr}^{-1}$ [69,70]. The magnetic fields on the neutron

stars in LMXBs are comparatively weak, lying in the range 10^8 G $\lesssim B_\star \lesssim 10^9$ G [20,70,71]. We substitute $\dot{M} = 10^{-8}\ M_\odot\ \mathrm{yr}^{-1}$ and $B_\star = 10^9$ G into Eq. (16) to maximize R_A and hence h_0^{eq}. The result is plotted as the orange curve in Fig. 5. Both torque-balance curves are plotted with $f_0 = 2f_\star$, i.e., an orthogonal biaxial rotor, which is a conventional assumption [30].

At the most sensitive subband starting at $f_0 = 194.6$ Hz, the electromagnetically constrained upper limit is a factor of about 1.2 below (3.1 above) the torque balance for $R = R_A$ ($R = R_\star$). The upper limits for a circularly polarized signal beat the $R = R_A$ torque-balance upper limit between 60 and 223 Hz, and the upper limits assuming an electromagnetically constrained inclination angle beat the $R = R_A$ torque-balance limit between 94 and 113 Hz.

The upper limits given in Fig. 5 are somewhat higher than those achieved by the most sensitive search to date, the O1 cross-correlation search, which has upper limits that are typically lower by a factor of approximately 1.5 [43]. A significant contributing factor to this is that the threshold S_{th} is set by assuming that the search at each binary orbital parameter is independent, while in fact there are significant correlations between adjacent points in search parameter space. These correlations are difficult to safely account for and so we make the conservative assumption that they are independent. Thus S_{th} is an overestimate of the threshold for a 1% false alarm probability, in turn overestimating the upper limits and making a direct comparison of the upper limits difficult.

This search also uses updated binary orbital parameter ranges, taking advantage of a more recent analysis of electromagnetic observations to produce a search better targeted at Sco X-1. Similarly, while the detector design is fundamentally unchanged between O1 and O2, various detector improvements mean that some instrumental lines have been removed or ameliorated, making this search sensitive to signals that would have been obscured by instrumental noise in searches using earlier datasets. The hidden Markov model is also designed with particular emphasis on robustness to spin wandering. Together, these three reasons mean that the search covers a slightly different region of parameter space compared to previous Sco X-1 searches.

VI. CONCLUSION

In this paper, we search the LIGO O2 dataset for continuous gravitational waves from the LMXB Sco X-1, using a hidden Markov model combined with the $\mathcal{J}$-statistic. We find no signal. The search band extends from 60 to 650 Hz. The sky location α, δ and orbital parameters P, a_0, and ϕ_a used for the matched filter are electromagnetically constrained; values are given in Table II. Monte Carlo simulations of spin-wandering signals injected into the LIGO O2 data imply frequentist 95% upper limits of $h_0^{95\%} = 3.47 \times 10^{-25}$, 1.92×10^{-25}, 1.42×10^{-25} for unknown, electromagnetically restricted ($\cos\iota \approx 0.72$), and circular polarizations respectively. The upper limits apply at 194.6 Hz, which is the most sensitive search frequency. For the electromagnetically restricted case, the limit is 3.1 times above, or 1.2 times below, the torque-balance limit, when the torque-balance lever arm is the stellar radius or the Alfvén radius respectively. Monte Carlo simulations are used to establish a detection threshold corresponding to a false alarm probability of $\alpha = 0.01$.

These results improve on the results from the previous HMM search described in Ref. [40], by using data from LIGO's second observing run, and by substituting the $\mathcal{J}$-statistic for the Bessel-weighted $\mathcal{F}$-statistic to track the phase of the orbital Doppler shift. As a result, the search in this paper is $\approx$2 times more sensitive compared to that in Ref. [40]. The analysis remains computationally efficient, requiring $\lesssim 3 \times 10^5$ GPU-hr for the search itself and $\lesssim 10^6$ GPU-hr for simulations to characterize the sensitivity and false alarm rate.

ACKNOWLEDGMENTS

The authors gratefully acknowledge the support of the United States National Science Foundation (NSF) for the construction and operation of the LIGO Laboratory and Advanced LIGO as well as the Science and Technology Facilities Council (STFC) of the United Kingdom, the Max-Planck-Society, and the State of Niedersachsen/Germany for support of the construction of Advanced LIGO and construction and operation of the GEO600 detector. Additional support for Advanced LIGO was provided by the Australian Research Council. The authors gratefully acknowledge the Italian Istituto Nazionale di Fisica Nucleare (INFN), the French Centre National de la Recherche Scientifique (CNRS), and the Foundation for Fundamental Research on Matter supported by the Netherlands Organisation for Scientific Research for the construction and operation of the Virgo detector and the creation and support of the EGO consortium. The authors also gratefully acknowledge research support from these agencies as well as by the Council of Scientific and Industrial Research of India, the Department of Science and Technology, India, the Science & Engineering Research Board, India, the Ministry of Human Resource Development, India, the Spanish Agencia Estatal de Investigación, the Vicepresidència i Conselleria d'Innovació, Recerca i Turisme and the Conselleria d'Educació i Universitat del Govern de les Illes Balears, the Conselleria d'Educació, Investigació, Cultura i Esport de la Generalitat Valenciana, the National Science Centre of Poland, the Swiss National Science Foundation, the Russian Foundation for Basic Research, the Russian Science Foundation, the European Commission, the European Regional Development Funds, the Royal Society, the Scottish Funding Council, the Scottish Universities

Physics Alliance, the Hungarian Scientific Research Fund, the Lyon Institute of Origins, the Paris Île-de-France Region, the National Research, Development and Innovation Office Hungary, the National Research Foundation of Korea, Industry Canada and the Province of Ontario through the Ministry of Economic Development and Innovation, the Natural Science and Engineering Research Council Canada, the Canadian Institute for Advanced Research, the Brazilian Ministry of Science, Technology, Innovations, and Communications, the International Center for Theoretical Physics South American Institute for Fundamental Research, the Research Grants Council of Hong Kong, the National Natural Science Foundation of China, the Leverhulme Trust, the Research Corporation, the Ministry of Science and Technology, Taiwan, and the Kavli Foundation. The authors gratefully acknowledge the support of the NSF, STFC, INFN, CNRS, Swinburne University of Technology, the National Collaborative Research Infrastructure Strategy of Australia, and the State of Niedersachsen/Germany for provision of computational resources. This work has been assigned LIGO Document No. LIGO-P1800208.

[1] K. Riles, Prog. Part. Nucl. Phys. **68**, 1 (2013).
[2] G. M. Harry (LIGO Scientific Collaboration), Classical Quantum Gravity **27**, 084006 (2010).
[3] J. Aasi, B. P. Abbott, R. Abbott, T. Abbott, M. R. Abernathy, K. Ackley, C. Adams, T. Adams, P. Addesso *et al.* (LIGO Scientific Collaboration), Classical Quantum Gravity **32**, 074001 (2015).
[4] F. Acernese *et al.* (Virgo Collaboration), Classical Quantum Gravity **32**, 024001 (2015).
[5] N. Andersson, V. Ferrari, D. I. Jones, K. D. Kokkotas, B. Krishnan, J. S. Read, L. Rezzolla, and B. Zink, Gen. Relativ. Gravit. **43**, 409 (2011).
[6] G. Ushomirsky, C. Cutler, and L. Bildsten, Mon. Not. R. Astron. Soc. **319**, 902 (2000).
[7] N. K. Johnson-McDaniel and B. J. Owen, Phys. Rev. D **88**, 044004 (2013).
[8] C. Cutler, Phys. Rev. D **66**, 084025 (2002).
[9] A. Mastrano, A. Melatos, A. Reisenegger, and T. Akgün, Mon. Not. R. Astron. Soc. **417**, 2288 (2011).
[10] P. D. Lasky and A. Melatos, Phys. Rev. D **88**, 103005 (2013).
[11] J. S. Heyl, Astrophys. J. Lett. **574**, L57 (2002).
[12] P. Arras, E. E. Flanagan, S. M. Morsink, A. K. Schenk, S. A. Teukolsky, and I. Wasserman, Astrophys. J. **591**, 1129 (2003).
[13] R. Bondarescu, S. A. Teukolsky, and I. Wasserman, Phys. Rev. D **79**, 104003 (2009).
[14] C. Peralta, A. Melatos, M. Giacobello, and A. Ooi, Astrophys. J. Lett. **644**, L53 (2006).
[15] C. A. van Eysden and A. Melatos, Classical Quantum Gravity **25**, 225020 (2008).
[16] M. F. Bennett, C. A. van Eysden, and A. Melatos, Mon. Not. R. Astron. Soc. **409**, 1705 (2010).
[17] A. Melatos, J. A. Douglass, and T. P. Simula, Astrophys. J. **807**, 132 (2015).
[18] D. Chakrabarty, E. H. Morgan, M. P. Muno, D. K. Galloway, R. Wijnands, M. van der Klis, and C. B. Markwardt, Nature (London) **424**, 42 (2003).
[19] G. B. Cook, S. L. Shapiro, and S. A. Teukolsky, Astrophys. J. **424**, 823 (1994).
[20] L. Bildsten, Astrophys. J. Lett. **501**, L89 (1998).
[21] J. Papaloizou and J. E. Pringle, Mon. Not. R. Astron. Soc. **184**, 501 (1978).
[22] R. V. Wagoner, Astrophys. J. **278**, 345 (1984).
[23] B. P. Abbott, R. Abbott, R. Adhikari, P. Ajith, B. Allen, G. Allen, R. S. Amin, S. B. Anderson, W. G. Anderson, M. A. Arain *et al.*, Rep. Prog. Phys. **72**, 076901 (2009).
[24] J. Abadie, B. P. Abbott, R. Abbott, T. D. Abbott, M. Abernathy, T. Accadia, F. Acernese, C. Adams, R. Adhikari, C. Affeldt *et al.* (LIGO Scientific and Virgo Collaborations), arXiv:1203.2674.
[25] B. P. Abbott, R. Abbott, T. D. Abbott, M. R. Abernathy, F. Acernese, K. Ackley, C. Adams, T. Adams, P. Addesso, R. X. Adhikari *et al.*, Phys. Rev. Lett. **116**, 131103 (2016).
[26] B. P. Abbott, R. Abbott, T. D. Abbott, M. R. Abernathy, F. Acernese, K. Ackley, C. Adams, T. Adams, P. Addesso, R. X. Adhikari *et al.*, Phys. Rev. Lett. **116**, 061102 (2016).
[27] B. P. Abbott, R. Abbott, T. D. Abbott, M. R. Abernathy, F. Acernese, K. Ackley, C. Adams, T. Adams, P. Addesso, R. X. Adhikari *et al.*, Phys. Rev. Lett. **116**, 241103 (2016).
[28] B. P. Abbott, R. Abbott, T. D. Abbott, S. Abraham, F. Acernese, K. Ackley, C. Adams, R. X. Adhikari *et al.* (LIGO Scientific and Virgo Collaborations), Phys. Rev. X **9**, 031040 (2019).
[29] B. P. Abbott, R. Abbott, T. D. Abbott, F. Acernese, K. Ackley, C. Adams, T. Adams, P. Addesso, R. X. Adhikari, V. B. Adya *et al.*, Phys. Rev. Lett. **119**, 161101 (2017).
[30] P. Jaranowski, A. Królak, and B. F. Schutz, Phys. Rev. D **58**, 063001 (1998).
[31] B. Abbott, R. Abbott, R. Adhikari, J. Agresti, P. Ajith, B. Allen, R. Amin, S. B. Anderson, W. G. Anderson, M. Arain *et al.*, Phys. Rev. D **76**, 082001 (2007).
[32] J. Aasi, B. P. Abbott, R. Abbott, T. Abbott, M. R. Abernathy, F. Acernese, K. Ackley, C. Adams, T. Adams, P. Addesso *et al.*, Phys. Rev. D **91**, 062008 (2015).
[33] E. Goetz and K. Riles, Classical Quantum Gravity **28**, 215006 (2011).
[34] J. Aasi, B. P. Abbott, R. Abbott, T. Abbott, M. R. Abernathy, T. Accadia, F. Acernese, K. Ackley, C. Adams, T. Adams *et al.*, Phys. Rev. D **90**, 062010 (2014).
[35] G. D. Meadors, E. Goetz, and K. Riles, Classical Quantum Gravity **33**, 105017 (2016).
[36] S. W. Ballmer, Classical Quantum Gravity **23**, S179 (2006).

[37] B. Abbott, R. Abbott, R. Adhikari, J. Agresti, P. Ajith, B. Allen, R. Amin, S. B. Anderson, W. G. Anderson, M. Arain *et al.*, Phys. Rev. D **76**, 082003 (2007).
[38] J. Abadie, B. P. Abbott, R. Abbott, M. Abernathy, T. Accadia, F. Acernese, C. Adams, R. Adhikari, P. Ajith, B. Allen, G. S. Allen, E. Amador Ceron, R. S. Amin, S. B. Anderson, W. G. Anderson, F. Antonucci *et al.* (LIGO Scientific and Virgo Collaboration), Phys. Rev. Lett. **107**, 271102 (2011).
[39] B. P. Abbott, R. Abbott, T. D. Abbott, M. R. Abernathy, F. Acernese, K. Ackley, C. Adams, T. Adams, P. Addesso, R. X. Adhikari *et al.*, Phys. Rev. Lett. **118**, 121102 (2017).
[40] B. P. Abbott, R. Abbott, T. D. Abbott, F. Acernese, K. Ackley, C. Adams, T. Adams, P. Addesso, R. X. Adhikari, V. B. Adya *et al.*, Phys. Rev. D **95**, 122003 (2017).
[41] J. T. Whelan, S. Sundaresan, Y. Zhang, and P. Peiris, Phys. Rev. D **91**, 102005 (2015).
[42] S. Dhurandhar, B. Krishnan, H. Mukhopadhyay, and J. T. Whelan, Phys. Rev. D **77**, 082001 (2008).
[43] B. P. Abbott, R. Abbott, T. D. Abbott, F. Acernese, K. Ackley, C. Adams, T. Adams, P. Addesso, R. X. Adhikari, V. B. Adya *et al.*, Astrophys. J. **847**, 47 (2017).
[44] C. Messenger, LIGO Report No. T1000195, 2011.
[45] G. D. Meadors, E. Goetz, K. Riles, T. Creighton, and F. Robinet, Phys. Rev. D **95**, 042005 (2017).
[46] M. deKool and U. Anzer, Mon. Not. R. Astron. Soc. **262**, 726 (1993).
[47] A. Baykal and H. Oegelman, Astron. Astrophys. **267**, 119 (1993).
[48] L. Bildsten, D. Chakrabarty, J. Chiu, M. H. Finger, D. T. Koh, R. W. Nelson, T. A. Prince, B. C. Rubin, D. M. Scott, M. Stollberg, B. A. Vaughan, C. A. Wilson, and R. B. Wilson, Astrophys. J. Suppl. Ser. **113**, 367 (1997).
[49] A. L. Watts, B. Krishnan, L. Bildsten, and B. F. Schutz, Mon. Not. R. Astron. Soc. **389**, 839 (2008).
[50] A. Mukherjee, C. Messenger, and K. Riles, Phys. Rev. D **97**, 043016 (2018).
[51] P. Leaci and R. Prix, Phys. Rev. D **91**, 102003 (2015).
[52] S. Suvorova, L. Sun, A. Melatos, W. Moran, and R. J. Evans, Phys. Rev. D **93**, 123009 (2016).
[53] S. Suvorova, P. Clearwater, A. Melatos, L. Sun, W. Moran, and R. J. Evans, Phys. Rev. D **96**, 102006 (2017).
[54] A. Viterbi, IEEE Trans. Inf. Theory **13**, 260 (1967).
[55] R. Prix and B. Krishnan, Classical Quantum Gravity **26**, 204013 (2009).
[56] C. F. Bradshaw, E. B. Fomalont, and B. J. Geldzahler, Astrophys. J. Lett. **512**, L121 (1999).
[57] L. Wang, D. Steeghs, D. K. Galloway, T. Marsh, and J. Casares, Mon. Not. R. Astron. Soc. **478**, 5174 (2018).
[58] E. B. Fomalont, B. J. Geldzahler, and C. F. Bradshaw, Astrophys. J. **558**, 283 (2001).
[59] C. Messenger, H. J. Bulten, S. G. Crowder, V. Dergachev, D. K. Galloway, E. Goetz, R. J. G. Jonker, P. D. Lasky, G. D. Meadors, A. Melatos, S. Premachandra, K. Riles, L. Sammut, E. H. Thrane, J. T. Whelan, and Y. Zhang, Phys. Rev. D **92**, 023006 (2015).
[60] L. Sammut, C. Messenger, A. Melatos, and B. J. Owen, Phys. Rev. D **89**, 043001 (2014).
[61] J. Aasi, B. P. Abbott, R. Abbott, T. Abbott, M. R. Abernathy, F. Acernese, K. Ackley, C. Adams, T. Adams, P. Addesso *et al.*, Phys. Rev. D **91**, 062008 (2015).
[62] D. Steeghs and J. Casares, Astrophys. J. **568**, 273 (2002).
[63] R. Prix, LIGO Report No. T0900149, 2011.
[64] LIGO Scientific Collaboration, LIGO Algorithm Library—LALSuite, free software (GPL) (2018).
[65] K. Wette, Phys. Rev. D **85**, 042003 (2012).
[66] B. Abbott, R. Abbott, R. Adhikari, J. Agresti, P. Ajith, B. Allen, R. Amin, S. B. Anderson, W. G. Anderson, M. Arain *et al.*, Phys. Rev. D **76**, 082001 (2007).
[67] P. B. Covas, A. Effler, E. Goetz, P. M. Meyers, A. Neunzert, M. Oliver, B. L. Pearlstone, V. J. Roma, R. M. S. Schofield, and V. B. Adya, Phys. Rev. D **97**, 082002 (2018).
[68] B. P. Abbott, R. Abbott, T. D. Abbott, M. R. Abernathy, F. Acernese, K. Ackley, C. Adams, T. Adams, P. Addesso, R. X. Adhikari *et al.*, Phys. Rev. Lett. **118**, 121101 (2017).
[69] H. Ritter and U. Kolb, Astron. Astrophys. **404**, 301 (2003).
[70] L. Sammut, Ph.D. thesis, University of Melbourne, 2015.
[71] A. Patruno and A. L. Watts, arXiv:1206.2727.

B. P. Abbott,[1] R. Abbott,[1] T. D. Abbott,[2] S. Abraham,[3] F. Acernese,[4,5] K. Ackley,[6] C. Adams,[7] R. X. Adhikari,[1] V. B. Adya,[8,9] C. Affeldt,[8,9] M. Agathos,[10] K. Agatsuma,[11] N. Aggarwal,[12] O. D. Aguiar,[13] L. Aiello,[14,15] A. Ain,[3] P. Ajith,[16] G. Allen,[17] A. Allocca,[18,19] M. A. Aloy,[20] P. A. Altin,[21] A. Amato,[22] A. Ananyeva,[1] S. B. Anderson,[1] W. G. Anderson,[23] S. V. Angelova,[24] S. Antier,[25] S. Appert,[1] K. Arai,[1] M. C. Araya,[1] J. S. Areeda,[26] M. Arène,[27] N. Arnaud,[25,28] S. Ascenzi,[29,30] G. Ashton,[6] S. M. Aston,[7] P. Astone,[31] F. Aubin,[32] P. Aufmuth,[9] K. AultONeal,[33] C. Austin,[2] V. Avendano,[34] A. Avila-Alvarez,[26] S. Babak,[35,27] P. Bacon,[27] F. Badaracco,[14,15] M. K. M. Bader,[36] S. Bae,[37] P. T. Baker,[38] F. Baldaccini,[39,40] G. Ballardin,[28] S. W. Ballmer,[41] S. Banagiri,[42] J. C. Barayoga,[1] S. E. Barclay,[43] B. C. Barish,[1] D. Barker,[44] K. Barkett,[45] S. Barnum,[12] F. Barone,[4,5] B. Barr,[43] L. Barsotti,[12] M. Barsuglia,[27] D. Barta,[46] J. Bartlett,[44] I. Bartos,[47] R. Bassiri,[48] A. Basti,[18,19] M. Bawaj,[49,40] J. C. Bayley,[43] M. Bazzan,[50,51] B. Bécsy,[52] M. Bejger,[27,53] I. Belahcene,[25] A. S. Bell,[43] D. Beniwal,[54] B. K. Berger,[48] G. Bergmann,[8,9] S. Bernuzzi,[55,56] J. J. Bero,[57] C. P. L. Berry,[58] D. Bersanetti,[59] A. Bertolini,[36] J. Betzwieser,[7] R. Bhandare,[60] J. Bidler,[26] I. A. Bilenko,[61] S. A. Bilgili,[38] G. Billingsley,[1] J. Birch,[7] R. Birney,[24] O. Birnholtz,[57] S. Biscans,[1,12] S. Biscoveanu,[6] A. Bisht,[9] M. Bitossi,[28,19] M. A. Bizouard,[25] J. K. Blackburn,[1] C. D. Blair,[7] D. G. Blair,[62] R. M. Blair,[44] S. Bloemen,[63] N. Bode,[8,9] M. Boer,[64] Y. Boetzel,[65] G. Bogaert,[64] F. Bondu,[66] E. Bonilla,[48]

R. Bonnand,[32] P. Booker,[8,9] B. A. Boom,[36] C. D. Booth,[67] R. Bork,[1] V. Boschi,[28] S. Bose,[68,3] K. Bossie,[7] V. Bossilkov,[62] J. Bosveld,[62] Y. Bouffanais,[27] A. Bozzi,[28] C. Bradaschia,[19] P. R. Brady,[23] A. Bramley,[7] M. Branchesi,[14,15] J. E. Brau,[69] T. Briant,[70] J. H. Briggs,[43] F. Brighenti,[71,72] A. Brillet,[64] M. Brinkmann,[8,9] V. Brisson,[25,a] P. Brockill,[23] A. F. Brooks,[1] D. D. Brown,[54] S. Brunett,[1] A. Buikema,[12] T. Bulik,[73] H. J. Bulten,[74,36] A. Buonanno,[35,75] D. Buskulic,[32] C. Buy,[27] R. L. Byer,[48] M. Cabero,[8,9] L. Cadonati,[76] G. Cagnoli,[22,77] C. Cahillane,[1] J. Calderón Bustillo,[6] T. A. Callister,[1] E. Calloni,[78,5] J. B. Camp,[79] W. A. Campbell,[6] M. Canepa,[80,59] K. C. Cannon,[81] H. Cao,[54] J. Cao,[82] E. Capocasa,[27] F. Carbognani,[28] S. Caride,[83] M. F. Carney,[58] G. Carullo,[18] J. Casanueva Diaz,[19] C. Casentini,[29,30] S. Caudill,[36] M. Cavaglià,[84] F. Cavalier,[25] R. Cavalieri,[28] G. Cella,[19] P. Cerdá-Durán,[20] G. Cerretani,[18,19] E. Cesarini,[85,30] O. Chaibi,[64] K. Chakravarti,[3] S. J. Chamberlin,[86] M. Chan,[43] S. Chao,[87] P. Charlton,[88] E. A. Chase,[58] E. Chassande-Mottin,[27] D. Chatterjee,[23] M. Chaturvedi,[60] B. D. Cheeseboro,[38] H. Y. Chen,[89] X. Chen,[62] Y. Chen,[45] H.-P. Cheng,[47] C. K. Cheong,[90] H. Y. Chia,[47] A. Chincarini,[59] A. Chiummo,[28] G. Cho,[91] H. S. Cho,[92] M. Cho,[75] N. Christensen,[64,93] Q. Chu,[62] S. Chua,[70] K. W. Chung,[90] S. Chung,[62] G. Ciani,[50,51] A. A. Ciobanu,[54] R. Ciolfi,[94,95] F. Cipriano,[64] A. Cirone,[80,59] F. Clara,[44] J. A. Clark,[76] P. Clearwater,[96] F. Cleva,[64] C. Cocchieri,[84] E. Coccia,[14,15] P.-F. Cohadon,[70] D. Cohen,[25] R. Colgan,[97] M. Colleoni,[98] C. G. Collette,[99] C. Collins,[11] L. R. Cominsky,[100] M. Constancio Jr.,[13] L. Conti,[51] S. J. Cooper,[11] P. Corban,[7] T. R. Corbitt,[2] I. Cordero-Carrión,[101] K. R. Corley,[97] N. Cornish,[52] A. Corsi,[83] S. Cortese,[28] C. A. Costa,[13] R. Cotesta,[35] M. W. Coughlin,[1] S. B. Coughlin,[67,58] J.-P. Coulon,[64] S. T. Countryman,[97] P. Couvares,[1] P. B. Covas,[98] E. E. Cowan,[76] D. M. Coward,[62] M. J. Cowart,[7] D. C. Coyne,[1] R. Coyne,[102] J. D. E. Creighton,[23] T. D. Creighton,[103] J. Cripe,[2] M. Croquette,[70] S. G. Crowder,[104] T. J. Cullen,[2] A. Cumming,[43] L. Cunningham,[43] E. Cuoco,[28] T. Dal Canton,[79] G. Dálya,[105] S. L. Danilishin,[8,9] S. D'Antonio,[30] K. Danzmann,[9,8] A. Dasgupta,[106] C. F. Da Silva Costa,[47] L. E. H. Datrier,[43] V. Dattilo,[28] I. Dave,[60] M. Davier,[25] D. Davis,[41] E. J. Daw,[107] D. DeBra,[48] M. Deenadayalan,[3] J. Degallaix,[22] M. De Laurentis,[78,5] S. Deléglise,[70] W. Del Pozzo,[18,19] L. M. DeMarchi,[58] N. Demos,[12] T. Dent,[8,9,108] R. De Pietri,[109,56] J. Derby,[26] R. De Rosa,[78,5] C. De Rossi,[22,28] R. DeSalvo,[110] O. de Varona,[8,9] S. Dhurandhar,[3] M. C. Díaz,[103] T. Dietrich,[36] L. Di Fiore,[5] M. Di Giovanni,[111,95] T. Di Girolamo,[78,5] A. Di Lieto,[18,19] B. Ding,[99] S. Di Pace,[112,31] I. Di Palma,[112,31] F. Di Renzo,[18,19] A. Dmitriev,[11] Z. Doctor,[89] F. Donovan,[12] K. L. Dooley,[67,84] S. Doravari,[8,9] I. Dorrington,[67] T. P. Downes,[23] M. Drago,[14,15] J. C. Driggers,[44] Z. Du,[82] J.-G. Ducoin,[25] P. Dupej,[43] S. E. Dwyer,[44] P. J. Easter,[6] T. B. Edo,[107] M. C. Edwards,[93] A. Effler,[7] P. Ehrens,[1] J. Eichholz,[1] S. S. Eikenberry,[47] M. Eisenmann,[32] R. A. Eisenstein,[12] R. C. Essick,[89] H. Estelles,[98] D. Estevez,[32] Z. B. Etienne,[38] T. Etzel,[1] M. Evans,[12] T. M. Evans,[7] V. Fafone,[29,30,14] H. Fair,[41] S. Fairhurst,[67] X. Fan,[82] S. Farinon,[59] B. Farr,[69] W. M. Farr,[11] E. J. Fauchon-Jones,[67] M. Favata,[34] M. Fays,[107] M. Fazio,[113] C. Fee,[114] J. Feicht,[1] M. M. Fejer,[48] F. Feng,[27] A. Fernandez-Galiana,[12] I. Ferrante,[18,19] E. C. Ferreira,[13] T. A. Ferreira,[13] F. Ferrini,[28] F. Fidecaro,[18,19] I. Fiori,[28] D. Fiorucci,[27] M. Fishbach,[89] R. P. Fisher,[41,115] J. M. Fishner,[12] M. Fitz-Axen,[42] R. Flaminio,[32,116] M. Fletcher,[43] E. Flynn,[26] H. Fong,[117] J. A. Font,[20,118] P. W. F. Forsyth,[21] J.-D. Fournier,[64] S. Frasca,[112,31] F. Frasconi,[19] Z. Frei,[105] A. Freise,[11] R. Frey,[69] V. Frey,[25] P. Fritschel,[12] V. V. Frolov,[7] P. Fulda,[47] M. Fyffe,[7] H. A. Gabbard,[43] B. U. Gadre,[3] S. M. Gaebel,[11] J. R. Gair,[119] L. Gammaitoni,[39] M. R. Ganija,[54] S. G. Gaonkar,[3] A. Garcia,[26] C. García-Quirós,[98] F. Garufi,[78,5] B. Gateley,[44] S. Gaudio,[33] G. Gaur,[120] V. Gayathri,[121] G. Gemme,[59] E. Genin,[28] A. Gennai,[19] D. George,[17] J. George,[60] L. Gergely,[122] V. Germain,[32] S. Ghonge,[76] Abhirup Ghosh,[16] Archisman Ghosh,[36] S. Ghosh,[23] B. Giacomazzo,[111,95] J. A. Giaime,[2,7] K. D. Giardina,[7] A. Giazotto,[19,a] K. Gill,[33] G. Giordano,[4,5] L. Glover,[110] P. Godwin,[86] E. Goetz,[44] R. Goetz,[47] B. Goncharov,[6] G. González,[2] J. M. Gonzalez Castro,[18,19] A. Gopakumar,[123] M. L. Gorodetsky,[61] S. E. Gossan,[1] M. Gosselin,[28] R. Gouaty,[32] A. Grado,[124,5] C. Graef,[43] M. Granata,[22] A. Grant,[43] S. Gras,[12] P. Grassia,[1] C. Gray,[44] R. Gray,[43] G. Greco,[71,72] A. C. Green,[11,47] R. Green,[67] E. M. Gretarsson,[33] P. Groot,[63] H. Grote,[67] S. Grunewald,[35] P. Gruning,[25] G. M. Guidi,[71,72] H. K. Gulati,[106] Y. Guo,[36] A. Gupta,[86] M. K. Gupta,[106] E. K. Gustafson,[1] R. Gustafson,[125] L. Haegel,[98] O. Halim,[15,14] B. R. Hall,[68] E. D. Hall,[12] E. Z. Hamilton,[67] G. Hammond,[43] M. Haney,[65] M. M. Hanke,[8,9] J. Hanks,[44] C. Hanna,[86] M. D. Hannam,[67] O. A. Hannuksela,[90] J. Hanson,[7] T. Hardwick,[2] K. Haris,[16] J. Harms,[14,15] G. M. Harry,[126] I. W. Harry,[35] C.-J. Haster,[117] K. Haughian,[43] F. J. Hayes,[43] J. Healy,[57] A. Heidmann,[70] M. C. Heintze,[7] H. Heitmann,[64] P. Hello,[25] G. Hemming,[28] M. Hendry,[43] I. S. Heng,[43] J. Hennig,[8,9] A. W. Heptonstall,[1] Francisco Hernandez Vivanco,[6] M. Heurs,[8,9] S. Hild,[43] T. Hinderer,[127,36,128] D. Hoak,[28] S. Hochheim,[8,9] D. Hofman,[22] A. M. Holgado,[17] N. A. Holland,[21] K. Holt,[7] D. E. Holz,[89] P. Hopkins,[67] C. Horst,[23] J. Hough,[43] E. J. Howell,[62] C. G. Hoy,[67] A. Hreibi,[64] E. A. Huerta,[17] D. Huet,[25] B. Hughey,[33] M. Hulko,[1] S. Husa,[98] S. H. Huttner,[43] T. Huynh-Dinh,[7] B. Idzkowski,[73] A. Iess,[29,30] C. Ingram,[54] R. Inta,[83] G. Intini,[112,31] B. Irwin,[114] H. N. Isa,[43] J.-M. Isac,[70] M. Isi,[1] B. R. Iyer,[16] K. Izumi,[44] T. Jacqmin,[70] S. J. Jadhav,[129] K. Jani,[76] N. N. Janthalur,[129] P. Jaranowski,[130] A. C. Jenkins,[131] J. Jiang,[47] D. S. Johnson,[17] A. W. Jones,[11] D. I. Jones,[132]

R. Jones,[43] R. J. G. Jonker,[36] L. Ju,[62] J. Junker,[8,9] C. V. Kalaghatgi,[67] V. Kalogera,[58] B. Kamai,[1] S. Kandhasamy,[84] G. Kang,[37] J. B. Kanner,[1] S. J. Kapadia,[23] S. Karki,[69] K. S. Karvinen,[8,9] R. Kashyap,[16] M. Kasprzack,[1] S. Katsanevas,[28] E. Katsavounidis,[12] W. Katzman,[7] S. Kaufer,[9] K. Kawabe,[44] N. V. Keerthana,[3] F. Kéfélian,[64] D. Keitel,[43] R. Kennedy,[107] J. S. Key,[133] F. Y. Khalili,[61] H. Khan,[26] I. Khan,[14,30] S. Khan,[8,9] Z. Khan,[106] E. A. Khazanov,[134] M. Khursheed,[60] N. Kijbunchoo,[21] Chunglee Kim,[135] J. C. Kim,[136] K. Kim,[90] W. Kim,[54] W. S. Kim,[137] Y.-M. Kim,[138] C. Kimball,[58] E. J. King,[54] P. J. King,[44] M. Kinley-Hanlon,[126] R. Kirchhoff,[8,9] J. S. Kissel,[44] L. Kleybolte,[139] J. H. Klika,[23] S. Klimenko,[47] T. D. Knowles,[38] P. Koch,[8,9] S. M. Koehlenbeck,[8,9] G. Koekoek,[36,140] S. Koley,[36] V. Kondrashov,[1] A. Kontos,[12] N. Koper,[8,9] M. Korobko,[139] W. Z. Korth,[1] I. Kowalska,[73] D. B. Kozak,[1] V. Kringel,[8,9] N. Krishnendu,[141] A. Królak,[142,143] G. Kuehn,[8,9] A. Kumar,[129] P. Kumar,[144] R. Kumar,[106] S. Kumar,[16] L. Kuo,[87] A. Kutynia,[142] S. Kwang,[23] B. D. Lackey,[35] K. H. Lai,[90] T. L. Lam,[90] M. Landry,[44] B. B. Lane,[12] R. N. Lang,[145] J. Lange,[57] B. Lantz,[48] R. K. Lanza,[12] A. Lartaux-Vollard,[25] P. D. Lasky,[6] M. Laxen,[7] A. Lazzarini,[1] C. Lazzaro,[51] P. Leaci,[112,31] S. Leavey,[8,9] Y. K. Lecoeuche,[44] C. H. Lee,[92] H. K. Lee,[146] H. M. Lee,[147] H. W. Lee,[136] J. Lee,[91] K. Lee,[43] J. Lehmann,[8,9] A. Lenon,[38] N. Leroy,[25] N. Letendre,[32] Y. Levin,[6,97] J. Li,[82] K. J. L. Li,[90] T. G. F. Li,[90] X. Li,[45] F. Lin,[6] F. Linde,[36] S. D. Linker,[110] T. B. Littenberg,[148] J. Liu,[62] X. Liu,[23] R. K. L. Lo,[90,1] N. A. Lockerbie,[24] L. T. London,[67] A. Longo,[149,150] M. Lorenzini,[14,15] V. Loriette,[151] M. Lormand,[7] G. Losurdo,[19] J. D. Lough,[8,9] C. O. Lousto,[57] G. Lovelace,[26] M. E. Lower,[152] H. Lück,[9,8] D. Lumaca,[29,30] A. P. Lundgren,[153] R. Lynch,[12] Y. Ma,[45] R. Macas,[67] S. Macfoy,[24] M. MacInnis,[12] D. M. Macleod,[67] A. Macquet,[64] F. Magaña-Sandoval,[41] L. Magaña Zertuche,[84] R. M. Magee,[86] E. Majorana,[31] I. Maksimovic,[151] A. Malik,[60] N. Man,[64] V. Mandic,[42] V. Mangano,[43] G. L. Mansell,[44,12] M. Manske,[23,21] M. Mantovani,[28] F. Marchesoni,[49,40] F. Marion,[32] S. Márka,[97] Z. Márka,[97] C. Markakis,[10,17] A. S. Markosyan,[48] A. Markowitz,[1] E. Maros,[1] A. Marquina,[101] S. Marsat,[35] F. Martelli,[71,72] I. W. Martin,[43] R. M. Martin,[34] D. V. Martynov,[11] K. Mason,[12] E. Massera,[107] A. Masserot,[32] T. J. Massinger,[1] M. Masso-Reid,[43] S. Mastrogiovanni,[112,31] A. Matas,[42,35] F. Matichard,[1,12] L. Matone,[97] N. Mavalvala,[12] N. Mazumder,[68] J. J. McCann,[62] R. McCarthy,[44] D. E. McClelland,[21] S. McCormick,[7] L. McCuller,[12] S. C. McGuire,[154] J. McIver,[1] D. J. McManus,[21] T. McRae,[21] S. T. McWilliams,[38] D. Meacher,[86] G. D. Meadors,[6] M. Mehmet,[8,9] A. K. Mehta,[16] J. Meidam,[36] A. Melatos,[96] G. Mendell,[44] R. A. Mercer,[23] L. Mereni,[22] E. L. Merilh,[44] M. Merzougui,[64] S. Meshkov,[1] C. Messenger,[43] C. Messick,[86] R. Metzdorff,[70] P. M. Meyers,[96] H. Miao,[11] C. Michel,[22] H. Middleton,[96] E. E. Mikhailov,[155] L. Milano,[78,5] A. L. Miller,[47] A. Miller,[112,31] M. Millhouse,[52] J. C. Mills,[67] M. C. Milovich-Goff,[110] O. Minazzoli,[64,156] Y. Minenkov,[30] A. Mishkin,[47] C. Mishra,[157] T. Mistry,[107] S. Mitra,[3] V. P. Mitrofanov,[61] G. Mitselmakher,[47] R. Mittleman,[12] G. Mo,[93] D. Moffa,[114] K. Mogushi,[84] S. R. P. Mohapatra,[12] M. Montani,[71,72] C. J. Moore,[10] D. Moraru,[44] G. Moreno,[44] S. Morisaki,[81] B. Mours,[32] C. M. Mow-Lowry,[11] Arunava Mukherjee,[8,9] D. Mukherjee,[23] S. Mukherjee,[103] N. Mukund,[3] A. Mullavey,[7] J. Munch,[54] E. A. Muñiz,[41] M. Muratore,[33] P. G. Murray,[43] A. Nagar,[85,158,159] I. Nardecchia,[29,30] L. Naticchioni,[112,31] R. K. Nayak,[160] J. Neilson,[110] G. Nelemans,[63,36] T. J. N. Nelson,[7] M. Nery,[8,9] A. Neunzert,[125] K. Y. Ng,[12] S. Ng,[54] P. Nguyen,[69] D. Nichols,[127,36] S. Nissanke,[127,36] F. Nocera,[28] C. North,[67] L. K. Nuttall,[153] M. Obergaulinger,[20] J. Oberling,[44] B. D. O'Brien,[47] G. D. O'Dea,[110] G. H. Ogin,[161] J. J. Oh,[137] S. H. Oh,[137] F. Ohme,[8,9] H. Ohta,[81] M. A. Okada,[13] M. Oliver,[98] P. Oppermann,[8,9] Richard J. Oram,[7] B. O'Reilly,[7] R. G. Ormiston,[42] L. F. Ortega,[47] R. O'Shaughnessy,[57] S. Ossokine,[35] D. J. Ottaway,[54] H. Overmier,[7] B. J. Owen,[83] A. E. Pace,[86] G. Pagano,[18,19] M. A. Page,[62] A. Pai,[121] S. A. Pai,[60] J. R. Palamos,[69] O. Palashov,[134] C. Palomba,[31] A. Pal-Singh,[139] Huang-Wei Pan,[87] B. Pang,[45] P. T. H. Pang,[90] C. Pankow,[58] F. Pannarale,[112,31] B. C. Pant,[60] F. Paoletti,[19] A. Paoli,[28] A. Parida,[3] W. Parker,[7,154] D. Pascucci,[43] A. Pasqualetti,[28] R. Passaquieti,[18,19] D. Passuello,[19] M. Patil,[143] B. Patricelli,[18,19] B. L. Pearlstone,[43] C. Pedersen,[67] M. Pedraza,[1] R. Pedurand,[22,162] A. Pele,[7] S. Penn,[163] C. J. Perez,[44] A. Perreca,[111,95] H. P. Pfeiffer,[35,117] M. Phelps,[8,9] K. S. Phukon,[3] O. J. Piccinni,[112,31] M. Pichot,[64] F. Piergiovanni,[71,72] G. Pillant,[28] L. Pinard,[22] M. Pirello,[44] M. Pitkin,[43] R. Poggiani,[18,19] D. Y. T. Pong,[90] S. Ponrathnam,[3] P. Popolizio,[28] E. K. Porter,[27] J. Powell,[152] A. K. Prajapati,[106] J. Prasad,[3] K. Prasai,[48] R. Prasanna,[129] G. Pratten,[98] T. Prestegard,[23] S. Privitera,[35] G. A. Prodi,[111,95] L. G. Prokhorov,[61] O. Puncken,[8,9] M. Punturo,[40] P. Puppo,[31] M. Pürrer,[35] H. Qi,[23] V. Quetschke,[103] P. J. Quinonez,[33] E. A. Quintero,[1] R. Quitzow-James,[69] F. J. Raab,[44] H. Radkins,[44] N. Radulescu,[64] P. Raffai,[105] S. Raja,[60] C. Rajan,[60] B. Rajbhandari,[83] M. Rakhmanov,[103] K. E. Ramirez,[103] A. Ramos-Buades,[98] Javed Rana,[3] K. Rao,[58] P. Rapagnani,[112,31] V. Raymond,[67] M. Razzano,[18,19] J. Read,[26] T. Regimbau,[32] L. Rei,[59] S. Reid,[24] D. H. Reitze,[1,47] W. Ren,[17] F. Ricci,[112,31] C. J. Richardson,[33] J. W. Richardson,[1] P. M. Ricker,[17] K. Riles,[125] M. Rizzo,[58] N. A. Robertson,[1,43] R. Robie,[43] F. Robinet,[25] A. Rocchi,[30] L. Rolland,[32] J. G. Rollins,[1] V. J. Roma,[69] M. Romanelli,[66] R. Romano,[4,5] C. L. Romel,[44] J. H. Romie,[7] K. Rose,[114] D. Rosińska,[164,53] S. G. Rosofsky,[17] M. P. Ross,[165] S. Rowan,[43] A. Rüdiger,[8,9,a] P. Ruggi,[28] G. Rutins,[166] K. Ryan,[44] S. Sachdev,[1] T. Sadecki,[44]

M. Sakellariadou,[131] L. Salconi,[28] M. Saleem,[141] A. Samajdar,[36] L. Sammut,[6] E. J. Sanchez,[1] L. E. Sanchez,[1] N. Sanchis-Gual,[20] V. Sandberg,[44] J. R. Sanders,[41] K. A. Santiago,[34] N. Sarin,[6] B. Sassolas,[22] P. R. Saulson,[41] O. Sauter,[125] R. L. Savage,[44] P. Schale,[69] M. Scheel,[45] J. Scheuer,[58] P. Schmidt,[63] R. Schnabel,[139] R. M. S. Schofield,[69] A. Schönbeck,[139] E. Schreiber,[8,9] B. W. Schulte,[8,9] B. F. Schutz,[67] S. G. Schwalbe,[33] J. Scott,[43] S. M. Scott,[21] E. Seidel,[17] D. Sellers,[7] A. S. Sengupta,[167] N. Sennett,[35] D. Sentenac,[28] V. Sequino,[29,30,14] A. Sergeev,[134] Y. Setyawati,[8,9] D. A. Shaddock,[21] T. Shaffer,[44] M. S. Shahriar,[58] M. B. Shaner,[110] L. Shao,[35] P. Sharma,[60] P. Shawhan,[75] H. Shen,[17] R. Shink,[168] D. H. Shoemaker,[12] D. M. Shoemaker,[76] S. ShyamSundar,[60] K. Siellez,[76] M. Sieniawska,[53] D. Sigg,[44] A. D. Silva,[13] L. P. Singer,[79] N. Singh,[73] A. Singhal,[14,31] A. M. Sintes,[98] S. Sitmukhambetov,[103] V. Skliris,[67] B. J. J. Slagmolen,[21] T. J. Slaven-Blair,[62] J. R. Smith,[26] R. J. E. Smith,[6] S. Somala,[169] E. J. Son,[137] B. Sorazu,[43] F. Sorrentino,[59] T. Souradeep,[3] E. Sowell,[83] A. P. Spencer,[43] A. K. Srivastava,[106] V. Srivastava,[41] K. Staats,[58] C. Stachie,[64] M. Standke,[8,9] D. A. Steer,[27] M. Steinke,[8,9] J. Steinlechner,[139,43] S. Steinlechner,[139] D. Steinmeyer,[8,9] S. P. Stevenson,[152] D. Stocks,[48] R. Stone,[103] D. J. Stops,[11] K. A. Strain,[43] G. Stratta,[71,72] S. E. Strigin,[61] A. Strunk,[44] R. Sturani,[170] A. L. Stuver,[171] V. Sudhir,[12] T. Z. Summerscales,[172] L. Sun,[1] S. Sunil,[106] J. Suresh,[3] P. J. Sutton,[67] B. L. Swinkels,[36] M. J. Szczepańczyk,[33] M. Tacca,[36] S. C. Tait,[43] C. Talbot,[6] D. Talukder,[69] D. B. Tanner,[47] M. Tápai,[122] A. Taracchini,[35] J. D. Tasson,[93] R. Taylor,[1] F. Thies,[8,9] M. Thomas,[7] P. Thomas,[44] S. R. Thondapu,[60] K. A. Thorne,[7] E. Thrane,[6] Shubhanshu Tiwari,[111,95] Srishti Tiwari,[123] V. Tiwari,[67] K. Toland,[43] M. Tonelli,[18,19] Z. Tornasi,[43] A. Torres-Forné,[173] C. I. Torrie,[1] D. Töyrä,[11] F. Travasso,[28,40] G. Traylor,[7] M. C. Tringali,[73] A. Trovato,[27] L. Trozzo,[174,19] R. Trudeau,[1] K. W. Tsang,[36] M. Tse,[12] R. Tso,[45] L. Tsukada,[81] D. Tsuna,[81] D. Tuyenbayev,[103] K. Ueno,[81] D. Ugolini,[175] C. S. Unnikrishnan,[123] A. L. Urban,[2] S. A. Usman,[67] H. Vahlbruch,[9] G. Vajente,[1] G. Valdes,[2] N. van Bakel,[36] M. van Beuzekom,[36] J. F. J. van den Brand,[74,36] C. Van Den Broeck,[36,176] D. C. Vander-Hyde,[41] J. V. van Heijningen,[62] L. van der Schaaf,[36] A. A. van Veggel,[43] M. Vardaro,[50,51] V. Varma,[45] S. Vass,[1] M. Vasúth,[46] A. Vecchio,[11] G. Vedovato,[51] J. Veitch,[43] P. J. Veitch,[54] K. Venkateswara,[165] G. Venugopalan,[1] D. Verkindt,[32] F. Vetrano,[71,72] A. Viceré,[71,72] A. D. Viets,[23] D. J. Vine,[166] J.-Y. Vinet,[64] S. Vitale,[12] T. Vo,[41] H. Vocca,[39,40] C. Vorvick,[44] S. P. Vyatchanin,[61] A. R. Wade,[1] L. E. Wade,[114] M. Wade,[114] R. Walet,[36] M. Walker,[26] L. Wallace,[1] S. Walsh,[23] G. Wang,[14,19] H. Wang,[11] J. Z. Wang,[125] W. H. Wang,[103] Y. F. Wang,[90] R. L. Ward,[21] Z. A. Warden,[33] J. Warner,[44] M. Was,[32] J. Watchi,[99] B. Weaver,[44] L.-W. Wei,[8,9] M. Weinert,[8,9] A. J. Weinstein,[1] R. Weiss,[12] F. Wellmann,[8,9] L. Wen,[62] E. K. Wessel,[17] P. Weßels,[8,9] J. W. Westhouse,[33] K. Wette,[21] J. T. Whelan,[57] B. F. Whiting,[47] C. Whittle,[12] D. M. Wilken,[8,9] D. Williams,[43] A. R. Williamson,[127,36] J. L. Willis,[1] B. Willke,[8,9] M. H. Wimmer,[8,9] W. Winkler,[8,9] C. C. Wipf,[1] H. Wittel,[8,9] G. Woan,[43] J. Woehler,[8,9] J. K. Wofford,[57] J. Worden,[44] J. L. Wright,[43] D. S. Wu,[8,9] D. M. Wysocki,[57] L. Xiao,[1] H. Yamamoto,[1] C. C. Yancey,[75] L. Yang,[113] M. J. Yap,[21] M. Yazback,[47] D. W. Yeeles,[67] Hang Yu,[12] Haocun Yu,[12] S. H. R. Yuen,[90] M. Yvert,[32] A. K. Zadrożny,[103,142] M. Zanolin,[33] T. Zelenova,[28] J.-P. Zendri,[51] M. Zevin,[58] J. Zhang,[62] L. Zhang,[1] T. Zhang,[43] C. Zhao,[62] M. Zhou,[58] Z. Zhou,[58] X. J. Zhu,[6] M. E. Zucker,[1,12] and J. Zweizig[1]

(LIGO Scientific Collaboration and Virgo Collaboration)

L. M. Dunn,[96] S. Suvorova,[96] R. J. Evans,[96] and W. Moran[96]

[1]*LIGO, California Institute of Technology, Pasadena, California 91125, USA*
[2]*Louisiana State University, Baton Rouge, Louisiana 70803, USA*
[3]*Inter-University Centre for Astronomy and Astrophysics, Pune 411007, India*
[4]*Università di Salerno, Fisciano, I-84084 Salerno, Italy*
[5]*INFN, Sezione di Napoli, Complesso Universitario di Monte S. Angelo, I-80126 Napoli, Italy*
[6]*OzGrav, School of Physics & Astronomy, Monash University, Clayton 3800, Victoria, Australia*
[7]*LIGO Livingston Observatory, Livingston, Louisiana 70754, USA*
[8]*Max Planck Institute for Gravitational Physics (Albert Einstein Institute), D-30167 Hannover, Germany*
[9]*Leibniz Universität Hannover, D-30167 Hannover, Germany*
[10]*University of Cambridge, Cambridge CB2 1TN, United Kingdom*
[11]*University of Birmingham, Birmingham B15 2TT, United Kingdom*
[12]*LIGO, Massachusetts Institute of Technology, Cambridge, Massachusetts 02139, USA*
[13]*Instituto Nacional de Pesquisas Espaciais, 12227-010 São José dos Campos, São Paulo, Brazil*
[14]*Gran Sasso Science Institute (GSSI), I-67100 L'Aquila, Italy*
[15]*INFN, Laboratori Nazionali del Gran Sasso, I-67100 Assergi, Italy*

[16]*International Centre for Theoretical Sciences, Tata Institute of Fundamental Research, Bengaluru 560089, India*
[17]*NCSA, University of Illinois at Urbana-Champaign, Urbana, Illinois 61801, USA*
[18]*Università di Pisa, I-56127 Pisa, Italy*
[19]*INFN, Sezione di Pisa, I-56127 Pisa, Italy*
[20]*Departamento de Astronomía y Astrofísica, Universitat de València, E-46100 Burjassot, València, Spain*
[21]*OzGrav, Australian National University, Canberra, Australian Capital Territory 0200, Australia*
[22]*Laboratoire des Matériaux Avancés (LMA), CNRS/IN2P3, F-69622 Villeurbanne, France*
[23]*University of Wisconsin-Milwaukee, Milwaukee, Wisconsin 53201, USA*
[24]*SUPA, University of Strathclyde, Glasgow G1 1XQ, United Kingdom*
[25]*LAL, Universite Paris-Sud, CNRS/IN2P3, Université Paris-Saclay, F-91898 Orsay, France*
[26]*California State University Fullerton, Fullerton, California 92831, USA*
[27]*APC, AstroParticule et Cosmologie, Université Paris Diderot, CNRS/IN2P3, CEA/Irfu, Observatoire de Paris, Sorbonne Paris Cité, F-75205 Paris Cedex 13, France*
[28]*European Gravitational Observatory (EGO), I-56021 Cascina, Pisa, Italy*
[29]*Università di Roma Tor Vergata, I-00133 Roma, Italy*
[30]*INFN, Sezione di Roma Tor Vergata, I-00133 Roma, Italy*
[31]*INFN, Sezione di Roma, I-00185 Roma, Italy*
[32]*Laboratoire d'Annecy de Physique des Particules (LAPP), Universite Grenoble Alpes, Université Savoie Mont Blanc, CNRS/IN2P3, F-74941 Annecy, France*
[33]*Embry-Riddle Aeronautical University, Prescott, Arizona 86301, USA*
[34]*Montclair State University, Montclair, New Jersey 07043, USA*
[35]*Max Planck Institute for Gravitational Physics (Albert Einstein Institute), D-14476 Potsdam-Golm, Germany*
[36]*Nikhef, Science Park 105, 1098 XG Amsterdam, Netherlands*
[37]*Korea Institute of Science and Technology Information, Daejeon 34141, South Korea*
[38]*West Virginia University, Morgantown, West Virginia 26506, USA*
[39]*Università di Perugia, I-06123 Perugia, Italy*
[40]*INFN, Sezione di Perugia, I-06123 Perugia, Italy*
[41]*Syracuse University, Syracuse, New York 13244, USA*
[42]*University of Minnesota, Minneapolis, Minnesota 55455, USA*
[43]*SUPA, University of Glasgow, Glasgow G12 8QQ, United Kingdom*
[44]*LIGO Hanford Observatory, Richland, Washington 99352, USA*
[45]*Caltech CaRT, Pasadena, California 91125, USA*
[46]*Wigner RCP, RMKI, H-1121 Budapest, Konkoly Thege Miklós út 29-33, Hungary*
[47]*University of Florida, Gainesville, Florida 32611, USA*
[48]*Stanford University, Stanford, California 94305, USA*
[49]*Università di Camerino, Dipartimento di Fisica, I-62032 Camerino, Italy*
[50]*Università di Padova, Dipartimento di Fisica e Astronomia, I-35131 Padova, Italy*
[51]*INFN, Sezione di Padova, I-35131 Padova, Italy*
[52]*Montana State University, Bozeman, Montana 59717, USA*
[53]*Nicolaus Copernicus Astronomical Center, Polish Academy of Sciences, 00-716, Warsaw, Poland*
[54]*OzGrav, University of Adelaide, Adelaide, South Australia 5005, Australia*
[55]*Theoretisch-Physikalisches Institut, Friedrich-Schiller-Universität Jena, D-07743 Jena, Germany*
[56]*INFN, Sezione di Milano Bicocca, Gruppo Collegato di Parma, I-43124 Parma, Italy*
[57]*Rochester Institute of Technology, Rochester, New York 14623, USA*
[58]*Center for Interdisciplinary Exploration & Research in Astrophysics (CIERA), Northwestern University, Evanston, Illinois 60208, USA*
[59]*INFN, Sezione di Genova, I-16146 Genova, Italy*
[60]*RRCAT, Indore, Madhya Pradesh 452013, India*
[61]*Faculty of Physics, Lomonosov Moscow State University, Moscow 119991, Russia*
[62]*OzGrav, University of Western Australia, Crawley, Western Australia 6009, Australia*
[63]*Department of Astrophysics/IMAPP, Radboud University Nijmegen, P.O. Box 9010, 6500 GL Nijmegen, Netherlands*
[64]*Artemis, Université Côte d'Azur, Observatoire Côte d'Azur, CNRS, CS 34229, F-06304 Nice Cedex 4, France*
[65]*Physik-Institut, University of Zurich, Winterthurerstrasse 190, 8057 Zurich, Switzerland*
[66]*Univ Rennes, CNRS, Institut FOTON—UMR6082, F-3500 Rennes, France*
[67]*Cardiff University, Cardiff CF24 3AA, United Kingdom*

[68]*Washington State University, Pullman, Washington 99164, USA*
[69]*University of Oregon, Eugene, Oregon 97403, USA*
[70]*Laboratoire Kastler Brossel, Sorbonne Université, CNRS, ENS-Université PSL, Collège de France, F-75005 Paris, France*
[71]*Università degli Studi di Urbino "Carlo Bo", I-61029 Urbino, Italy*
[72]*INFN, Sezione di Firenze, I-50019 Sesto Fiorentino, Firenze, Italy*
[73]*Astronomical Observatory Warsaw University, 00-478 Warsaw, Poland*
[74]*VU University Amsterdam, 1081 HV Amsterdam, Netherlands*
[75]*University of Maryland, College Park, Maryland 20742, USA*
[76]*School of Physics, Georgia Institute of Technology, Atlanta, Georgia 30332, USA*
[77]*Université Claude Bernard Lyon 1, F-69622 Villeurbanne, France*
[78]*Università di Napoli "Federico II", Complesso Universitario di Monte S.Angelo, I-80126 Napoli, Italy*
[79]*NASA Goddard Space Flight Center, Greenbelt, Maryland 20771, USA*
[80]*Dipartimento di Fisica, Università degli Studi di Genova, I-16146 Genova, Italy*
[81]*RESCEU, University of Tokyo, Tokyo, 113-0033, Japan*
[82]*Tsinghua University, Beijing 100084, China*
[83]*Texas Tech University, Lubbock, Texas 79409, USA*
[84]*The University of Mississippi, University, Mississippi 38677, USA*
[85]*Museo Storico della Fisica e Centro Studi e Ricerche "Enrico Fermi," I-00184 Roma, Italyrico Fermi, I-00184 Roma, Italy*
[86]*The Pennsylvania State University, University Park, Pennsylvania 16802, USA*
[87]*National Tsing Hua University, Hsinchu City, 30013 Taiwan, Republic of China*
[88]*Charles Sturt University, Wagga Wagga, New South Wales 2678, Australia*
[89]*University of Chicago, Chicago, Illinois 60637, USA*
[90]*The Chinese University of Hong Kong, Shatin, New Territories, Hong Kong*
[91]*Seoul National University, Seoul 08826, South Korea*
[92]*Pusan National University, Busan 46241, South Korea*
[93]*Carleton College, Northfield, Minnesota 55057, USA*
[94]*INAF, Osservatorio Astronomico di Padova, I-35122 Padova, Italy*
[95]*INFN, Trento Institute for Fundamental Physics and Applications, I-38123 Povo, Trento, Italy*
[96]*OzGrav, University of Melbourne, Parkville, Victoria 3010, Australia*
[97]*Columbia University, New York, New York 10027, USA*
[98]*Universitat de les Illes Balears, IAC3—IEEC, E-07122 Palma de Mallorca, Spain*
[99]*Université Libre de Bruxelles, Brussels 1050, Belgium*
[100]*Sonoma State University, Rohnert Park, California 94928, USA*
[101]*Departamento de Matemáticas, Universitat de València, E-46100 Burjassot, València, Spain*
[102]*University of Rhode Island, Kingston, Rhode Island 02881, USA*
[103]*The University of Texas Rio Grande Valley, Brownsville, Texas 78520, USA*
[104]*Bellevue College, Bellevue, Washington 98007, USA*
[105]*MTA-ELTE Astrophysics Research Group, Institute of Physics, Eötvös University, Budapest 1117, Hungary*
[106]*Institute for Plasma Research, Bhat, Gandhinagar 382428, India*
[107]*The University of Sheffield, Sheffield S10 2TN, United Kingdom*
[108]*IGFAE, Campus Sur, Universidade de Santiago de Compostela, 15782 Spain*
[109]*Dipartimento di Scienze Matematiche, Fisiche e Informatiche, Università di Parma, I-43124 Parma, Italy*
[110]*California State University, Los Angeles, 5151 State University Drive, Los Angeles, California 90032, USA*
[111]*Università di Trento, Dipartimento di Fisica, I-38123 Povo, Trento, Italy*
[112]*Università di Roma "La Sapienza", I-00185 Roma, Italy*
[113]*Colorado State University, Fort Collins, Colorado 80523, USA*
[114]*Kenyon College, Gambier, Ohio 43022, USA*
[115]*Christopher Newport University, Newport News, Virginia 23606, USA*
[116]*National Astronomical Observatory of Japan, 2-21-1 Osawa, Mitaka, Tokyo 181-8588, Japan*
[117]*Canadian Institute for Theoretical Astrophysics, University of Toronto, Toronto, Ontario M5S 3H8, Canada*
[118]*Observatori Astronòmic, Universitat de València, E-46980 Paterna, València, Spain*
[119]*School of Mathematics, University of Edinburgh, Edinburgh EH9 3FD, United Kingdom*

[120]*Institute Of Advanced Research, Gandhinagar 382426, India*
[121]*Indian Institute of Technology Bombay, Powai, Mumbai 400 076, India*
[122]*University of Szeged, Dóm tér 9, Szeged 6720, Hungary*
[123]*Tata Institute of Fundamental Research, Mumbai 400005, India*
[124]*INAF, Osservatorio Astronomico di Capodimonte, I-80131, Napoli, Italy*
[125]*University of Michigan, Ann Arbor, Michigan 48109, USA*
[126]*American University, Washington, D.C. 20016, USA*
[127]*GRAPPA, Anton Pannekoek Institute for Astronomy and Institute of High-Energy Physics, University of Amsterdam, Science Park 904, 1098 XH Amsterdam, Netherlands*
[128]*Delta Institute for Theoretical Physics, Science Park 904, 1090 GL Amsterdam, Netherlands*
[129]*Directorate of Construction, Services & Estate Management, Mumbai 400094 India*
[130]*University of Białystok, 15-424 Biał ystok, Poland*
[131]*King's College London, University of London, London WC2R 2LS, United Kingdom*
[132]*University of Southampton, Southampton SO17 1BJ, United Kingdom*
[133]*University of Washington Bothell, Bothell, Washington 98011, USA*
[134]*Institute of Applied Physics, Nizhny Novgorod, 603950, Russia*
[135]*Ewha Womans University, Seoul 03760, South Korea*
[136]*Inje University Gimhae, South Gyeongsang 50834, South Korea*
[137]*National Institute for Mathematical Sciences, Daejeon 34047, South Korea*
[138]*Ulsan National Institute of Science and Technology, Ulsan 44919, South Korea*
[139]*Universität Hamburg, D-22761 Hamburg, Germany*
[140]*Maastricht University, P.O. Box 616, 6200 MD Maastricht, Netherlands*
[141]*Chennai Mathematical Institute, Chennai 603103, India*
[142]*NCBJ, 05-400 Świerk-Otwock, Poland*
[143]*Institute of Mathematics, Polish Academy of Sciences, 00656 Warsaw, Poland*
[144]*Cornell University, Ithaca, New York 14850, USA*
[145]*Hillsdale College, Hillsdale, Michigan 49242, USA*
[146]*Hanyang University, Seoul 04763, South Korea*
[147]*Korea Astronomy and Space Science Institute, Daejeon 34055, South Korea*
[148]*NASA Marshall Space Flight Center, Huntsville, Alabama 35811, USA*
[149]*Dipartimento di Matematica e Fisica, Università degli Studi Roma Tre, I-00146 Roma, Italy*
[150]*INFN, Sezione di Roma Tre, I-00146 Roma, Italy*
[151]*ESPCI, CNRS, F-75005 Paris, France*
[152]*OzGrav, Swinburne University of Technology, Hawthorn, Victoria 3122, Australia*
[153]*University of Portsmouth, Portsmouth, PO1 3FX, United Kingdom*
[154]*Southern University and A&M College, Baton Rouge, Louisiana 70813, USA*
[155]*College of William and Mary, Williamsburg, Virginia 23187, USA*
[156]*Centre Scientifique de Monaco, 8 quai Antoine Ier, MC-98000, Monaco*
[157]*Indian Institute of Technology Madras, Chennai 600036, India*
[158]*INFN Sezione di Torino, Via P. Giuria 1, I-10125 Torino, Italy*
[159]*Institut des Hautes Etudes Scientifiques, F-91440 Bures-sur-Yvette, France*
[160]*IISER-Kolkata, Mohanpur, West Bengal 741252, India*
[161]*Whitman College, 345 Boyer Avenue, Walla Walla, Washington 99362 USA*
[162]*Université de Lyon, F-69361 Lyon, France*
[163]*Hobart and William Smith Colleges, Geneva, New York 14456, USA*
[164]*Janusz Gil Institute of Astronomy, University of Zielona Góra, 65-265 Zielona Góra, Poland*
[165]*University of Washington, Seattle, Washington 98195, USA*
[166]*SUPA, University of the West of Scotland, Paisley PA1 2BE, United Kingdom*
[167]*Indian Institute of Technology, Gandhinagar Ahmedabad Gujarat 382424, India*
[168]*Université de Montréal/Polytechnique, Montreal, Quebec H3T 1J4, Canada*
[169]*Indian Institute of Technology Hyderabad, Sangareddy, Khandi, Telangana 502285, India*
[170]*International Institute of Physics, Universidade Federal do Rio Grande do Norte, Natal RN 59078-970, Brazil*
[171]*Villanova University, 800 Lancaster Avenue, Villanova, Pennsylvania 19085, USA*
[172]*Andrews University, Berrien Springs, Michigan 49104, USA*
[173]*Max Planck Institute for Gravitationalphysik (Albert Einstein Institute), D-14476 Potsdam-Golm, Germany*

[174]*Università di Siena, I-53100 Siena, Italy*
[175]*Trinity University, San Antonio, Texas 78212, USA*
[176]*Van Swinderen Institute for Particle Physics and Gravity, University of Groningen, Nijenborgh 4, 9747 AG Groningen, Netherlands*

[a]Deceased.